# Cancer cell CCR2 orchestrates suppression of the adaptive immune response

Miriam R. Fein[1,2,*], Xue-Yan He[1,*], Ana S. Almeida[1,#], Emilis Bružas[1,4], Arnaud Pommier[1], Ran Yan[1,4], Anaïs Eberhardt[1,3], Douglas T. Fearon[1,5,6], Linda Van Aelst[1], John E. Wilkinson[7], Camila O. dos Santos[1], Mikala Egeblad[1†]

[1]Cold Spring Harbor Laboratory, Cold Spring Harbor, NY, 11724, USA
[2]Graduate Program in Genetics, Stony Brook University, Stony Brook, NY, 11794, USA
[3]Département de Biologie, École Normale Supérieure de Lyon, 69007 Lyon, France
[4]Watson School of Biological Sciences, Cold Spring Harbor, NY, 11724, USA
[5]Cancer Research UK Cambridge Institute, University of Cambridge, Li Ka Shing Centre, Cambridge CB2 0RE, UK
[6]Weill Cornell Medical College, New York, NY, 10021, USA
[7]Departments of Molecular & Integrative Physiology and Internal Medicine, University of Michigan, Ann Arbor, MI, 48109, USA
*These authors contributed equally
[#] Current address: APC Microbiome and School of Microbiology, University College Cork, Cork, Ireland

[†]***Corresponding author:***
Dr. Mikala Egeblad
Cold Spring Harbor Laboratory
1 Bungtown Road
Cold Spring Harbor, NY 11724, USA
Phone: 516 367 6852
Email: egeblad@cshl.edu
ORCID: orcid.org/0000-0002-3371-1445

**Running title**

CCR2 signaling in cancer cells causes immune evasion

**Summary**

C-C chemokine receptor type 2 (CCR2) expressed on monocytes facilitates their recruitment to tumors. Here, CCR2 signaling in cancer cells is shown to suppress immune control of tumors, in part by reducing CD103+ dendritic cell recruitment.

**ABSTRACT**

C-C chemokine receptor type 2 (CCR2) is expressed on monocytes and facilitates their recruitment to tumors. Although breast cancer cells also express CCR2, its functions in these cells are unclear. We found that *Ccr2* deletion in cancer cells led to reduced tumor growth and ~2-fold longer survival in an orthotopic isograft breast cancer mouse model. Deletion of *Ccr2* in cancer cells resulted in multiple alterations associated with better immune control: increased infiltration and activation of cytotoxic T lymphocytes (CTLs) and CD103+ cross-presenting dendritic cells (DCs), as well as upregulation of MHC class I and downregulation of checkpoint regulator PD-L1 on the cancer cells. Pharmacological inhibition of CCR2 increased cancer cell sensitivity to CTLs and enabled cancer cells to induce DC maturation toward the CD103+ subtype. Consistently, *Ccr2*$^{-/-}$ cancer cells did not induce immune suppression in *Batf3*$^{-/-}$ mice lacking the CD103+ DC subtype. Our results establish that CCR2 signaling in cancer cells can orchestrate suppression of the immune response.

## INTRODUCTION

Tumors escape immune control via multiple mechanisms (Dunn et al., 2002; Dunn et al., 2004). These mechanisms include cancer cell-intrinsic changes that alter how the cancer cell is recognized by the immune system and extrinsic changes that suppress immune cell activities. For example, cancer cells can intrinsically decrease the surface expression of major histocompatibility complex (MHC) class I, making them effectively invisible to cytotoxic T lymphocytes (CTLs) (Garrido et al., 2016). Moreover, cancer cells can upregulate programmed cell death ligand 1 (PD-L1/B7-H1), which binds and activates the PD-1 receptor on effector T cells, causing T cell anergy, which ultimately protects cancer cells against T cell-mediated killing (Chen et al., 2016a). Extrinsic mechanisms include the downregulation of co-stimulatory molecules (*e.g.*, CD86) on antigen-presenting cells; the secretion of cytokines that directly inhibit CTLs; and the recruitment of regulatory T cells and myeloid-derived suppressor cells (MDSCs) (Igney and Krammer, 2002). In contrast, infiltration of CD103+ dendritic cells (DCs) in mice, phenotypically similar to CD141+ DCs in humans (Hildner et al., 2008), has emerged as a mechanism by which tumors may be kept under immune control. CD103+ DCs are highly efficient at acquiring and processing exogenous antigens, which they directly present on MHC class I molecules to CD8+ CTLs. Even a modest accumulation of CD103+ DCs in tumors has been associated with improved immune-mediated tumor control (Broz et al., 2014; Roberts et al., 2016).

Chemokine receptors mediate the recruitment of immune cells to sites of inflammation and to tumors. C-C chemokine receptor type 2 (CCR2) is expressed by several bone marrow-derived cell types (including inflammatory monocytes, myeloid precursor cells, and immature DCs), as well as B and T lymphocytes (Lim et al., 2016). CCR2-expressing cells are recruited to sites of inflammation by C-C chemokine ligand 2 (CCL2) (Deshmane et al., 2009). Chemotherapy treatment promotes CCR2-dependent infiltration of tumor-promoting myeloid cells to murine mammary tumors (Nakasone et al., 2012), and

CCL2/CCR2-mediated recruitment of CCR2+ inflammatory monocytes to the lung has been shown to promote breast cancer extravasation and metastasis in mice models (Qian et al., 2011). Furthermore, elevated levels of CCL2 in tumors and in serum are associated with advanced disease and poor prognosis in breast carcinoma patients (Lebrecht et al., 2004; Lebrecht et al., 2001; Soria and Ben-Baruch, 2008). These findings have sparked interest in targeting the CCR2 pathway to modulate the innate immune response for therapeutic benefit in cancer. However, CCR2 is also expressed by breast cancer cells, and activation of CCR2 by CCL2 can induce cancer cell migration and survival through Smad3-, p42/44MAPK-, and Rho GTPase-mediated signaling (Fang et al., 2012). *In vivo*, the potential role(s) of CCR2 signaling in cancer cells have not been well investigated, largely because they were thought to be minor compared to the roles of CCR2 in myeloid cells.

In this study, we report that CCR2 signaling in cancer cells plays a significant role in regulating the immune response to murine breast tumors. We show that CCR2 in cancer cells supports immune escape by inhibiting CD103+ DC infiltration and maturation and by suppressing cytotoxic T cell activity. CCR2 expression on cancer cells represents a previously uncharacterized mechanism for immune suppression. Thus, our data support the notion that the CCL2/CCR2 axis is an important immune modulatory pathway in cancer, utilized by both immune cells and cancer cells to orchestrate immune suppression.

## RESULTS

### CCR2 in cancer cells promotes primary tumor growth in an orthotopic, isograft breast cancer mouse model

To investigate the potential effects of CCR2 on breast tumor growth and metastasis, we crossed *Ccr2*$^{-/-}$ mice (Boring et al., 1997) with mouse mammary tumor virus - polyoma middle T (MMTV-PyMT) mice, a model of luminal B breast cancer (Guy et al., 1992; Lin et al., 2003). The *Ccr2* genotype did not influence normal mammary gland development (**Fig. S1a**) or tumor onset (**Fig. 1a**); however, loss of even one allele of *Ccr2* significantly reduced tumor growth rates (**Fig. 1b**). Consistently, survival time was significantly longer for the MMTV-PyMT;*Ccr2*$^{-/-}$ and MMTV-PyMT;*Ccr2*$^{+/-}$ mice compared to that of the MMTV-PyMT;*Ccr2*$^{+/+}$ mice (**Fig. 1c**). In addition, we noted that tumors of MMTV-PyMT;*Ccr2*$^{-/-}$ and MMTV-PyMT;*Ccr2*$^{+/-}$ mice were more cystic, with reduced solid areas, than those of MMTV-PyMT;*Ccr2*$^{+/+}$ mice (**Fig. S1b, c**)

The importance of CCR2 signaling for monocyte recruitment is well understood, but CCR2 is also expressed by human breast cancer cells (Fang et al., 2012). In accordance with this report, we detected *Ccr2* mRNA and CCR2 protein in the cancer cells of the tumors developing in MMTV-PyMT;*Ccr2*$^{+/+}$ mice (**Fig. 1d**, **e**), and, using RNA FISH, demonstrated that *Ccr2* mRNA is expressed by *Krt18*-positive breast cancer cells (Fig. **S1d**). To determine the relative contributions of cancer cell vs. host CCR2 to tumor growth, we isolated primary cancer cells (purity >90%; **Fig. S1e**) from MMTV-PyMT;*Ccr2*$^{+/+}$ and MMTV-PyMT;*Ccr2*$^{-/-}$ mice and transplanted them orthotopically to mammary fat pads of either *Ccr2*$^{+/+}$ or *Ccr2*$^{-/-}$ syngeneic host mice (**Fig. 1f**). Loss of *Ccr2* in the host did not alter tumor growth, consistent with our previous report (Nakasone et al., 2012). However, loss of *Ccr2* in cancer cells significantly reduced tumor growth rates, leading to ~2-fold longer survival (**Fig. 1g, h**). *Ccr2* mRNA levels of *Ccr2*$^{+/-}$ cancer cells were lower than those of *Ccr2*$^{+/+}$ cancer cells (**Fig. S1f**), and tumors derived from *Ccr2*$^{+/-}$

cancer cells exhibited the same slow growth as tumors derived from *Ccr2*$^{-/-}$ cancer cells (**Fig. S1g**). This result suggests that a threshold level of CCR2 expression in MMTV-PyMT cancer cells accelerates tumor growth.

CCR2+ inflammatory monocytes and macrophages can promote breast cancer metastasis (Muller et al., 2001; Qian et al., 2011). However, the overall metastatic burden in the lung—the primary site of metastasis in the MMTV-PyMT model—was very variable in MMTV-PyMT;*Ccr2*$^{+/+}$mice and was not significantly different from that of MMTV-PyMT;*Ccr2*$^{-/-}$ mice (**Fig. S1h**). There were also no significant differences in the number of metastatic foci (representing seeding density) related to the *Ccr2* genotype (**Fig. S1i**). However, we found that the metastatic foci were larger in the lungs of MMTV-PyMT;*Ccr2*$^{+/+}$ mice than in the lungs of MMTV-PyMT;*Ccr2*$^{-/-}$ mice (**Fig. S1j**), suggesting that CCR2 promotes the growth of secondary lesions.

### *Ccr2* expression in cancer cells is associated with poor differentiation and reduced apoptosis sensitivity

Tumors derived from transplanted *Ccr2*$^{+/+}$ or *Ccr2*$^{-/-}$ MMTV-PyMT cancer cells were markedly different at the histological level (**Fig. 2a**), similarly to autochthonous tumors (**Fig. S1b, c**). Tumors originating from *Ccr2*$^{+/+}$ cancer cells consisted entirely of microlobules that contained sheets of large, neoplastic epithelial cells. The microlobules were surrounded by small amounts of fibrovascular stroma containing dense collagen, which is characteristic of poorly differentiated MMTV-PyMT tumors. The neoplastic cells had round to oval nuclei, prominent nucleoli, scant cytoplasm, and indistinct cell borders, typical of undifferentiated cells. In contrast, tumors originating from *Ccr2*$^{-/-}$ cancer cells were more differentiated. In many areas, the cancer cells contained lipid vacuoles of various sizes. These tumors also had large cystic areas lined by a single or double layer of small, polarized epithelial cells, and the lumina were filled

with proteinaceous secretions (**Fig. 2a**). Furthermore, tumors originating from *Ccr2*$^{-/-}$ cancer cells had a reduced percentage of solid areas compared to those originating from *Ccr2*$^{+/+}$ cancer cells (**Fig. 2b**).

To understand why tumors from *Ccr2*$^{-/-}$ cancer cells grew more slowly than tumors from *Ccr2*$^{+/+}$ cancer cells, we next examined the rates of proliferation and apoptosis in tumors collected during the phase when *Ccr2*$^{-/-}$ tumors were growth-restricted, 5-6 weeks post-transplantation. There was no difference in the percentage of proliferating cells as determined by nuclear Ki67 staining (**Fig. 2c**), and primary *Ccr2*$^{+/+}$ and *Ccr2*$^{-/-}$ cancer cells also proliferated at similarly *in vitro* (**Fig. 2d**). However, we found a higher percentage of cells undergoing apoptosis in tumors derived from *Ccr2*$^{-/-}$ cancer cells compared to those derived from *Ccr2*$^{+/+}$ cancer cells, as determined by TUNEL staining (**Fig. 2e**). Furthermore, while the epithelial cell populations isolated from both tumor types were equally viable under normal cell culture conditions, *Ccr2*$^{-/-}$ cancer cells were more sensitive to serum-free conditions (**Fig. 2f**), consistent with a previous study showing that CCR2 signaling can protect cancer cells from apoptosis induced by serum starvation (Fang et al., 2012).

**_Ccr2_$^{-/-}$ cancer cells have increased expression of interferon (IFN) response genes as well as genes involved in MHC class I antigen presentation**

To determine which pathways in *Ccr2*$^{-/-}$ cancer cells lead to reduced tumor growth and increased cell death, we isolated cancer cells from *Ccr2*$^{+/+}$ and *Ccr2*$^{-/-}$ transplanted tumors formed in wild-type hosts for equal amounts of time and performed transcriptome profiling by RNA-seq. Overall, 520 genes were differentially expressed (adjusted p-value <0.05), ~40% of which were upregulated in *Ccr2*$^{-/-}$ cancer cells compared to *Ccr2*$^{+/+}$ cancer cells. Among the differentially expressed genes, we detected upregulation of MHC class I (H2-K1) and Tap1, two genes required for antigen presentation, as well as IFI27, an IFN response gene, in the *Ccr2*$^{-/-}$ cancer cells (**Fig. 3a**). Vimentin, which is found in poorly differentiated

epithelial cells and in mesenchymal cells, was downregulated in *Ccr2*$^{-/-}$ cancer cells. This is consistent with a previous study describing a mesenchymal phenotype in CCR2-expressing cancer cells (Hu et al. 2019). Additionally, gene set enrichment analysis (GSEA) showed robust expression enrichment of the IFN-γ response hallmark gene set, which includes antigen processing and presentation genes, in *Ccr2*$^{-/-}$ cancer cells compared to *Ccr2*$^{+/+}$ cancer cells (**Fig. 3b**). We also observed a pronounced luminal gene expression signature in the *Ccr2*$^{-/-}$ cancer cells (**Fig. 3b**), in agreement with the noted histological differences (**Fig. 2a, b**). Consistently, gene ontology (GO) term analysis revealed altered expression of pathways involved in 1) regulation of the adaptive immune system and in 2) response to immune-mediated cell killing (**Fig. 3c**).

**Cancer cell CCR2 promotes immune suppression**

The increased expression of genes associated with IFN response and antigen presentation, together with the prolonged growth delay and increased apoptosis in tumors from *Ccr2*$^{-/-}$ cancer cells, are consistent with an ongoing adaptive immune response in the tumors. We therefore determined CCR2 expression in cancer cells correlated with differences in intratumoral immune cell infiltration by flow cytometry (for gating strategy, see **Fig. S2**). There were significantly more CD8+ CTLs and fewer CD4+ helper T cells in tumors derived from *Ccr2*$^{-/-}$ cancer cells compared to tumors derived from *Ccr2*$^{+/+}$ cancer cells (**Fig. 4a**), with no overall change in CD3+ T cell infiltration (**Fig. S3a**). Increased infiltration of CD8+ cells into tumors derived from *Ccr2*$^{-/-}$ cancer cells was also evident by immunofluorescence (**Fig. 4b, c**). PD-1 is a surface co-inhibitory receptor expressed by effector CD8+ T cells (Chen et al., 2016a), and its expression was increased on CD8+ T cells from tumors derived from *Ccr2*$^{-/-}$ cancer cells (**Fig. 4d**). CTLs kill, in part, through the release of granzyme B, a process that requires lysosomal-associated membrane protein 1 (LAMP-1, also known as Cluster of Differentiation 107a, CD107a). In tumors derived from

*Ccr2*$^{-/-}$ cancer cells, LAMP-1 was increased on the cell surface of CD8+ T cells (**Fig. 4e**), while granzyme B levels were reduced in CD8+ T cells (**Fig. 4f**), suggesting increased levels of prior CD8+ degranulation and hence cytotoxic activity. Rregulatory T lymphocytes (CD4+FoxP3+ regulatory T cells), were more abundant in tumors from *Ccr2*$^{-/-}$ cancer cells (**Fig. S3b**).

Tumors derived from *Ccr2*$^{-/-}$ cancer cells had multiple differences in the adaptive immune cell infiltrate, all consistent with an active immune response. Therefore, we tested whether adaptive immunity contributed to the differences in growth rates between the *Ccr2*$^{+/+}$ and *Ccr2*$^{-/-}$ tumors by transplanting cancer cells in parallel into T cell-deficient nude athymic or fully immunocompetent syngeneic host mice (**Fig. 5a**). In immunocompetent hosts, tumors derived from *Ccr2*$^{-/-}$ cancer cells grew significantly more slowly than tumors derived from *Ccr2*$^{+/+}$ cancer cells (**Fig. 5b**), as previously observed (**Fig. 1g**). In contrast, in T cell-deficient hosts, the *Ccr2*$^{-/-}$ tumors grew almost as rapidly as the *Ccr2*$^{+/+}$ tumors, with no significant difference in tumor volume at endpoint (**Fig. 5c**). Consistently, tumors derived from *Ccr2*$^{-/-}$ cancer cells grew as rapidly as tumors derived from *Ccr2*$^{+/+}$ cancer cells when CD8+ T cells were depleted using an antibody-based strategy (**Fig. S3c**). Furthermore, in the athymic hosts, tumors derived from *Ccr2*$^{-/-}$ cancer cells no longer had more apoptotic cells than tumors derived from *Ccr2*$^{+/+}$ cancer cells (**Fig. 5d**). Interestingly, the differentiated histological phenotype of the tumors from the *Ccr2*$^{-/-}$ cancer cells was maintained in T cell-deficient mice (**Fig. 5e**). Thus, the histological differences were not the result of an altered adaptive immune response. Together, these data demonstrate that CCR2 expressed by cancer cells enables tumors to escape the adaptive immune response.

We next hypothesized that the reduced growth of tumors derived from *Ccr2*$^{-/-}$ cancer cells could be a result of increased sensitivity to CTL-induced cell death, given that *Ccr2*$^{-/-}$ cancer cells showed increased cell death in serum-free conditions and that tumors grew normally when CD8+ T cells were depleted. To test this possibility, we used the MMTV-PyMT-chOVA model (Engelhardt et al., 2012),

which is driven by the PyMT oncogene and co-expresses ovalbumin (OVA) as a model tumor antigen and mCherry for tracking. We generated MMTV-PyMT-chOVA;*Ccr2*$^{+/+}$ and MMTV-PyMT-chOVA;*Ccr2*$^{-/-}$ mice, and found that just as in MMTV-PyMT;*Ccr2*$^{-/-}$ tumors, MMTV-PyMT-chOVA;*Ccr2*$^{-/-}$ tumors grew more slowly than MMTV-PyMT-chOVA;*Ccr2*$^{+/+}$ tumors (**Fig. 6a**). When primary cancer cells were isolated and challenged with activated CTLs isolated from OT-1 mice, which recognize cells that present MHC class I-bound OVA peptide, we found that MMTV-PyMT-chOVA;*Ccr2*$^{-/-}$ cancer cells were approximately twice as sensitive to OVA-specific CTLs compared to MMTV-PyMT-chOVA;*Ccr2*$^{+/+}$ cancer cells (**Fig. 6b**). This difference also persisted when exogenous OVA peptides were added to the cancer cells (**Fig. 6b**). Upon treatment with a pharmacological CCR2 antagonist (RS 102895 hydrochloride (Mitchell et al., 2013)), MMTV-PyMT-chOVA;*Ccr2*$^{+/+}$ cancer cells became as sensitive to the OVA-specific CTLs as MMTV-PyMT-chOVA;*Ccr2*$^{-/-}$ cancer cells (**Fig. 6c**). In contrast, the CCR2 antagonist had no effect on the specific cytotoxicity of CTLs against MMTV-PyMT-chOVA;*Ccr2*$^{-/-}$ cancer cells.

To test if *Ccr2* expression in cancer cells also regulated sensitivity to CTLs *in vivo,* we measured the clonal expansion of T cells, an indicator of active proliferation of antigen-specific T cells, by sequencing the complementarity determining region 3 (CDR3) region of the T cell receptor (TCR) β chain. We found that clonality, a value corresponding to the extent of clonal expansion of T cells (**Fig. 6d**), was significantly higher in tumors from *Ccr2*$^{-/-}$ cancer cells than in tumors from *Ccr2*$^{+/+}$ cancer cells (**Fig. 6e**), while there was no difference in clonality in the spleens of these groups of mice (**Fig. 6f**). These results suggested that tumor-recognizing CTLs were actively expanding due to antigen recognition in tumors from *Ccr2*$^{-/-}$ cancer cells, but that this expansion did not alter the systemic T cell response. Both *Ccr2*$^{+/+}$ and *Ccr2*$^{-/-}$ cancer cells express the PyMT tumor antigen, and transplanted *Ccr2*$^{+/+}$ cancer cells formed tumors at the same rate regardless of whether *Ccr2*$^{+/+}$ or *Ccr2*$^{-/-}$ cancer cells were transplanted in the

contralateral mammary fat pad (**Fig. S3d**). Together, these results suggest that the expression of CCR2 by cancer cells enables the tumors to establish a locally immune-suppressive microenvironment by compromising antigen-specific effector T cell expansion and directly inhibiting T cell cytotoxicity.

**Cancer cell CCR2 alters MHC class I and PD-L1 expression**

CCR2 signaling can activate STAT transcription factors in cancer cells (Chen et al., 2015; Izumi et al., 2013), and altered STAT1 or STAT3 signaling in cancer cells can in turn lead to expression of pro-inflammatory genes (Ahn et al., 2017; Jones et al., 2016). Therefore, we tested whether STAT activation was different between tumors derived from *Ccr2*$^{+/+}$ and *Ccr2*$^{-/-}$ cancer cells. We found no consistent differences between the activation of STAT1, STAT3, or p65/RELA when whole tumor lysate was assayed by Western blot (**Fig. 7a**). By immunohistochemistry, we found that the tumors contained patches of cancer cells with high expression of phopho-STAT1, with more of these patches in the tumors from *Ccr2*$^{-/-}$ than from *Ccr2*$^{+/+}$ cancer cells (**Fig. 7b, c**). No difference was observed for phospho-STAT3. These data are consistent with the possible involvement of STAT1 signaling as a regulator of an immune-suppressed microenvironment.

We next sought to understand how CCR2 signaling in cancer cells resulted in more efficient immune suppression. RNA-seq analysis of the cancer cells showed increased expression of genes involved in antigen presentation in the *Ccr2*$^{-/-}$ tumors (**Fig. 3c**). Consistently, we found high levels of MHC class I on cancer cells in MMTV-PyMT-chOVA;*Ccr2*$^{-/-}$ mice and more variable, low to intermediate, levels on cancer cells in MMTV-PyMT-chOVA;*Ccr2*$^{+/+}$ mice (**Fig. 8a**). Similarly, when cancer cells were transplanted to immunocompetent host mice, the levels of MHC class I were higher in tumors derived from *Ccr2*$^{-/-}$ cancer cells compared to those derived from *Ccr2*$^{+/+}$ cells, as shown by immunohistochemistry (**Fig. 8b**). However, in T cell-deficient hosts, MHC class I levels were similar in

tumors derived from both *Ccr2*$^{+/+}$ and *Ccr2*$^{-/-}$ cancer cells (**Fig. 8c**). These data suggest that MHC class I expression is not directly regulated by CCR2 signaling in the cancer cells, but rather is regulated by the different immune responses between these tumors.

PD-L1 is a potent suppressor of T cell activation and proliferation and is expressed on many types of cancer cells (Freeman et al., 2000). Cancer cells from *Ccr2*$^{+/+}$ tumors expressed significantly higher PD-L1 levels compared to *Ccr2*$^{-/-}$ cancer cells (**Fig. 8d**). Since both MHC class I and PD-L1 are IFN-γ response genes, we compared *Ifn*-g mRNA levels during the early tumor phase (3 weeks post-transplantation), and found significantly higher levels of *Ifn*-g in whole tumor lysate from tumors derived from *Ccr2*$^{-/-}$ tumors by RT-PCR (**Fig. S4a**). *In situ* hybridization revealed that the majority of the *Ifn*-g mRNA was expressed by infiltrating CD8+ T cells, and that *Ifn*-g mRNA levels were more variable at the growth-restricted phase of tumors than in the early tumor establishment phase (**Fig. S4b, c, d**). *In vitro,* recombinant IFN-γ treatment resulted in similar upregulation of *Pd-l1* mRNA levels in *Ccr2*$^{+/+}$ and *Ccr2*$^{-/-}$ cancer cells (**Fig. 8e**). Thus, our data suggest that *Ccr2*$^{-/-}$ cancer cells were still able to respond to IFN-γ by upregulating PD-L1. Lastly, we tested whether antibody-based PD-L1 blockade would alleviate immune suppression of the MMTV-PyMT tumors *in vivo*. However, anti-PD-L1 therapy had no significant effect on the growth of *Ccr2*$^{+/+}$ tumors, nor on the low PD-L1-expressing *Ccr2*$^{-/-}$ tumors (**Fig. 8f**). Thus, although reduced PD-L1 likely contributed to an increased sensitivity to CTLs in tumors from *Ccr2*$^{-/-}$ cancer cells, targeting PD-L1 expression was insufficient to reduce growth of the *Ccr2*$^{+/+}$ tumors.

**Cancer cell CCR2 prevents the infiltration of cross-presenting CD103+ DCs**

Next, we examined infiltration levels of immune populations that might be involved in immune suppression. There was no difference in CD11b+MHC class II+F4/80+ macrophages between tumors derived from *Ccr2*$^{+/+}$ and *Ccr2*$^{-/-}$ cancer cells (**Fig. S4e**). There were, however, significantly fewer

CD11b+MHC class II- myeloid cells in tumors from *Ccr2*$^{-/-}$ cancer cells (**Fig. S4f**). This population includes subsets of MDSCs, immature myeloid cells with immune-suppressive activity. Specifically, we found fewer granulocytes and granulocytic MDSCs (CD11b+CD11c-Ly6G+Ly6C$^{low}$ cells) and more inflammatory monocytes and myeloid MDSCs (CD11b+CD11c-Ly6G-Ly6C$^{high}$ cells) in tumors from *Ccr2*$^{-/-}$ cancer cells than from *Ccr2*$^{+/+}$ cancer cells (**Fig. S4g, h**).

Since DCs are critical for T cell activation, we performed immunohistochemistry for CD11c+, a marker of DCs, and observed more infiltrating CD11c+ cells in tumors derived from *Ccr2*$^{-/-}$ cancer cells than in those derived from *Ccr2*$^{+/+}$ cancer cells (**Fig. 9a**). Futhermore, we observed more than double the level of CD103+ DCs—a DC subtype that is very efficient at cross-presenting antigens to CD8+ T cells—in tumors derived from *Ccr2*$^{-/-}$ cancer cells than in those from *Ccr2*$^{+/+}$ cancer cells (**Fig. 9b**). The number of CD103+ DCs was also increased in the draining lymph nodes (dLNs) for these tumors (**Fig. 9c**). Using RT-PCR from whole tumor lysate and a panel of markers previously shown to be enriched on CD103+ DCs (Broz et al., 2014), we detected more mRNA for *Cd11c* and from activation markers, including *Cd80*, *Cd86, and Il12b* (**Fig. 9d**). Consistently, DCs in tumors from *Ccr2*$^{-/-}$ cancer cells displayed higher levels of CD86, a surface marker upregulated on activated DCs, determined by flow cytometry (**Fig. 9e**). There were also more CD103+ DCs in the spontaneously developing tumors in MMTV-PyMT;*Ccr2*$^{-/-}$ hosts compared to MMTV-PyMT;*Ccr2*$^{+/+}$ hosts (**Fig. S4i**). The difference in CD103+ DC numbers was already apparent in the dLNs two days after injection of irradiated cancer cells into the mammary fat pad (**Fig. 9f**), suggesting a direct signal from the cancer cells. However, there was no significant difference in infiltration of CD103+ DCs in immune-compromised mice (**Fig. 9g**). This finding suggests that a feedback loop between T cells and DCs is critical for CD103+ DC recruitment to the tumors.

We next asked whether a factor secreted by *Ccr2*$^{-/-}$ cancer cells was responsible for DC maturation toward the CD103+ DC subtype. Indeed, when bone marrow-derived cells were cultured with conditioned

medium from *Ccr2*$^{-/-}$ or *Ccr2*$^{+/+}$ cancer cells, a significantly higher percentage of CD11c+ cells were positive for CD103+ in the former condition, despite the same total number of DCs (**Fig. 10a**). Furthermore, the percentage of CD103+CD11c+ cells also increased by using conditioned medium from *Ccr2*$^{+/+}$ cancer cells treated with the CCR2 inhibitor (**Fig. 10b**). Adding the CCR2 inhibitor directly to the bone marrow-derived cultures did not by itself increase the percentage of CD103+ cells (**Fig. 10b**). Flt3 ligand and granulocyte-macrophage colony-stimulating factor (GM-CSF) can both stimulate DC maturation toward the CD103+ subtype (Broz et al., 2014). Consistently, we found more mRNA for both *Flt3l* and *Csf2* (coding for GM-CSF) in the tumors derived from *Ccr2*$^{-/-}$ cancer cells compared to those derived from *Ccr2*$^{+/+}$ cancer cells by RT-PCR (**Figs. 9d, 10c**). Protein arrays showed that the levels of two CCR2 ligands, CCL2 and CCL12, and most other cytokines were similar between MMTV-PyMT;*Ccr2*$^{+/+}$ and MMTV-PyMT;*Ccr2*$^{-/-}$ tumors (**Fig. S5a**), while IL-16 and granulocyte colony-stimulating factor (G-CSF) were significantly lower in the MMTV-PyMT;*Ccr2*$^{-/-}$ tumors at the protein level. When secretions from overnight cultures of the cancer cells under serum-free conditions were analyzed, CCL2, CCL12, G-CSF, and IL-16 were secreted to the same degree by *Ccr2*$^{+/+}$ and *Ccr2*$^{-/-}$ cancer cells (**Fig. S5b**). Lastly, to test the importance of the CD103+ DCs in regulating an immune-controlling microenvironment, we transplanted *Ccr2*$^{-/-}$ and *Ccr2*$^{+/+}$ cancer cells into *Batf3*$^{-/-}$ mice, which lack the basic leucine zipper transcription factor ATF-like 3 (BATF3) critical for CD103+ DC maturation. In these mice, the growth of *Ccr2*$^{-/-}$ cancer cell-derived tumors was equivalent to that of *Ccr2*$^{+/+}$ cancer cell-derived tumors (**Fig. 10d**), and as expected, the percentage of infiltrating CD103+ DCs was significantly reduced (**Fig. 10e**). Furthermore, CD8+ T cell infiltration, as well as expression of CD107a and PD-1 by T cells, were lower in tumors derived from *Ccr2*$^{-/-}$ cancer cells transplanted into *Batf3*$^{-/-}$ mice (**Figs. 10f, g, h**).Altogether, our findings support the notion that CD103+ DC and CD8+ T cells act in a positive feedback loop to regulate tumor immunity, and that interfering with one population can result in changes in to the other.

**DISCUSSION**

The tumor-promoting effects of CCR2 are well-documented. However, they have mostly been attributed to CCR2-expressing immune and other host cells (Lim et al., 2016; Nakasone et al., 2012; Qian et al., 2009; Qian et al., 2011; Wolf et al., 2012). Yet, CCR2 is also upregulated on breast cancer cells in a subset of breast cancers and this upregulation has been correlated with decreased survival (Labovsky et al., 2017). The expression of CCR2 by cancer cells has been proposed to promote tumor growth through increased motility and invasion, cell proliferation, and cell survival (Fang et al., 2012; Hu et al., 2019; Lu et al., 2006). Here, we show that in the MMTV-PyMT mouse model, CCR2 signaling in cancer cells helps breast tumors establish a locally immune-suppressive microenvironment. Compared to tumors from *Ccr2*$^{+/+}$ cancer cells, the tumors from *Ccr2*$^{-/-}$ cancer cells have higher infiltration of CD103+ DCs and activated CD8+ T cells, as well as lower infiltration of granulocytic MDSCs. Furthermore, the *Ccr2*$^{-/-}$ cancer cells have higher surface levels of MHC class I and lower levels of PD-L1. It is likely the combination of all of these changes that results in more effective immune surveillance of the *Ccr2*$^{-/-}$ cancer cells and reduced growth of tumors from these cells (**Fig. 10f**). To our knowledge, the ability of cancer cell CCR2 signaling to orchestrate tumor immune suppression has not previously been recognized.

One of the most notable changes in the tumor immune microenvironment caused by targeting cancer cell CCR2 expression was the increased levels of both CD103+ DCs and CD8+ T cells in tumors derived from *Ccr2*$^{-/-}$ cancer cells. The infiltration of these two cell populations was apparently connected. In athymic mice lacking mature CD8+ cells but not CD103+ cells, CD103+ DC infiltration was no longer elevated in tumors derived from *Ccr2*$^{-/-}$ cancer cells compared to those derived from *Ccr*$^{+/+}$cells. Conversely, in *Batf3*$^{-/-}$ mice, which lack the transcription factor BATF3 required for CD103+ DC development, CD8+ T cell infiltration was equally low for tumors derived from *Ccr2*$^{+/+}$ and *Ccr2*$^{-/-}$ tumors. These observations are consistent with several other recent reports intimately linking the function

of CD103+ DCs and CD8+ T cells in tumors. First, CD103+ DCs has been shown to secrete chemokines mediating T cell infiltration, including CXCL9 and -10 (de Mingo Pulido et al., 2018; Spranger et al., 2017). Second, secretion of IL-12 from CD103+ DCs was shown to stimulate CD8+ T cell function (Ruffell et al., 2014). Our data support these previous studies, showing not only a link between the CD103+ DC and CD8+ T cell infiltration, but also increased *Cxcl9* and *Il-12b* mRNA in tumors derived from *Ccr2*$^{-/-}$ cancer cells. Altogether, these data support the conclusion that regulation of CD103+ DC infiltration is a critical step in tumor immune surveillance (Broz et al., 2014; Meyer et al., 2018; Roberts et al., 2016). Our data further suggest that CCR2 signaling regulates the secretion of factors from the cancer cells that affects the polarization of DCs to the CD103+ subtype. Several factors have been proposed to induce the polarization of CD103+ DCs, including Flt3L and GM-CSF (Mayer et al., 2014), and consistently, mRNA levels for both of these factors were higher in tumors derived from *Ccr2*$^{-/-}$ cancer cells than from *Ccr2*$^{+/+}$ cancer cells. However, it is unclear if Flt3L and GM-CSF could be solely responsible for the difference in CD103+ DC infiltration between tumors from *Ccr2*$^{+/+}$ or from *Ccr2*$^{-/-}$ cancer cells. A recent study reported that G-CSF secreted from MMTV-PyMT cancer cells can inhibit the differentiation of CD103+ DCs by downregulating interferon regulatory factor-8 in DC progenitors (Meyer et al., 2018). Interestingly, G-CSF mRNAlevels were lower in MMTV-PyMT;*Ccr2*$^{-/-}$ tumors compared to MMTV-PyMT;*Ccr2*$^{+/+}$ tumors, although secretion of G-CSF from isolated cancer cells was not reduced, suggesting that altered secretion is not a direct effect of CCR2 signaling in cancer cells. *Ccr2*$^{-/-}$ cancer cells had distinct expression of a wide range of genes, including many that were consistent with an IFN response. Among these, increased surface expression of MHC class I might explain why *Ccr2*$^{-/-}$ cancer cells are more sensitive to T cell-mediated killing than *Ccr2*$^{+/+}$ cancer cells. However, since *Ccr2*$^{+/+}$ cancer cells did not downregulate MHC class I in T cell-deficient nude athymic mice, we speculate that MHC class I expression is not directly regulated by CCR2 signaling in the cancer cells. Rather, the altered

expression of IFN response genes, including MHC class I, may be an indirect result of an immune response in the tumors. Altogether, we propose that the cancer cells act on CD103+ DCs, leading to a feedbakc loop between CD103+ DCs and CD8+ T cells, two immune cell types with highly interconnected functions.

Our study has several translational implications. First, our findings provide a possible explanation as to why CCR2 overexpression in breast cancer cells is associated with decreased survival (Labovsky et al., 2017). Second, results from an open-label, non-randomized phase I trial using a CCR2 inhibitor against locally invasive pancreatic cancer suggest that the inhibitor enhanced chemotherapy response, reduced macrophage infiltration, and induced an anti-tumor adaptive immune response (Nywening et al., 2016). Our data suggest that the potential clinical benefits of CCR2 inhibitors might be caused by the combined inhibition of CCR2 signaling in both stromal and cancer cells. Interestingly, the loss of even one *Ccr2* allele was sufficient to reduce tumor growth in our study, suggesting that partial inhibition of CCR2 could result in clinical benefit. It is unclear why *Ccr2*$^{+/-}$ cancer cells phenocopy the *Ccr2*$^{-/-}$ cancer cells, but this phenomenon could be due to reduced dimerization of CCR2 in *Ccr2*$^{+/-}$ cancer cells, consistent with a prior report (Rodriguez-Frade et al., 1999), or because surpassing a threshold level of CCR2 signaling is required to induce immune suppression. Finally, recombinant G-CSF and GM-CSF are routinely given with certain types of chemotherapy to support the bone marrow and reduce the risk of lethal febrile neutropenia (Mehta et al., 2015). However, our data support prior studies suggesting that these cytokines play complex roles in regulating the immune response against tumors: they appear to have opposing effects on CD103+ DC differentiation, with GM-CSF stimulating CD103+ DC differentiation (Greter et al., 2012; Mayer et al., 2014) and G-CSF inhibiting this process (Meyer et al., 2018). Although GM-CSF secretion in the tumor microenvironment potentially enhances immune responses against tumors by stimulating CD103+ DC differentiation, this cytokine can also mobilize immune-suppressive MDSCs,

leading to suppression of an anti-tumor immune response (Bayne et al., 2012; Pylayeva-Gupta et al., 2012). Therefore, exploring other approaches than administration of recombinant GM-CSF and G-CSF to specifically boost CD103+ DC maturation could be an important future translational direction, and determining the exact mechanism that causes inhibition of cancer cell CCR2 signaling to promote CD103+ maturation may provide insights into how this occurs.

We found that tumor onset was similar between MMTV-PyMT;*Ccr2*$^{+/+}$ and MMTV-PyMT;*Ccr2*$^{-/-}$ mice, while tumor growth was slower. These data are in agreement with a prior report studying the tumor growth in MTMV-*Neu* mice, where mice null for *Ccl2*, the ligand for CCR2, or mice treated with a pharmacological CCR2 inhibitor also had similar tumor onset and but reduced tumor growth rates, as did mice treated with a CCR2 inhibitor (Chen et al., 2016b). However, unexpectedly, MMTV-*Neu* mice lacking *Ccr2* had accelerated, and not reduced, tumor growth in this study, and the authors speculated that this could be due to abnormal differentiation of the monocytes in these mice or unintentional effects of the genetic targeting of *Ccr2*. There are several possible explanations for the difference between our result using MMTV-PyMT;*Ccr2*$^{-/-}$ mice and that of the MMTv-Neu;*Ccr2*$^{-/-}$ mice in the previous publication. First, tumors of the MMTV-PyMT mice have more stromal components than tumors of the MMTV-*Neu* model. Second, the genetic background of mice used in our experiments was C57BL/6, while it was BALB/c in the case of the MMTV-*Neu* model. Finally, our tumor transplantation experiments strongly suggest that the tumor growth phenotype in our model is caused by CCR2 expression by cancer cells, but it is not clear whether cancer cells in the MMTV-Neu model express CCR2, or whether the phenotype is due to effects from stromal cells.

Despite the data suggesting that CCR2 inhibition has beneficial effects in cancer treatment, some studies have raised serious concerns about targeting the CCR2 ligand. Cessation of anti-CCL2 therapy resulted in increased pulmonary metastasis and decreased survival in a murine model of breast cancer,

due to rapid mobilization of CCR2-expressing monocytes into circulation immediately upon cessation of therapy (Bonapace et al., 2014). Therefore, CCR2 inhibition likely will have to be used in combination with other therapies to maximize the eradication of existing cancer cells and to avoid complications of discontinuing the inhibition. In summary, the divergent results across mouse models, genetic backgrounds, and variable experimental approaches to targeting CCL2 or CCR2 highlights that the effects of targeting this axis can depend on context such as tumor subtype, genetic background, and intratumoral cell types.

Our findings support the notion that the CCL2/CCR2 axis is an immune modulatory pathway in cancer, but with the added layer of complexity that cancer cells can hijack this chemokine receptor pathway to orchestrate immune suppression. In this study, we have focused on characterizing the cellular mechanisms responsible for the novel link between cancer cell CCR2 signaling and tumor immune suppression. Preclinical experiments suggest that CCR2 targeting strategies can have detrimental effects, including the promotion of metastasis (Bonapace et al., 2014; Li et al., 2013). Therefore, future work that identifies the precise mechanisms by which CCR2 signaling in cancer cells induces immune suppression in breast cancer may set the stage for developing novel immune modulatory therapies. There are ongoing clinical trials using pharmacological inhibitors of CCR2 in cancer patients, and our data suggest that the potential effects of inhibiting CCR2 signaling in cancer cells should be taken into account when interpreting the results from these trials.

## MATERIALS AND METHODS

### Mice

*Ccr2*$^{-/-}$, *Batf3*$^{-/-}$, and OT-1 mice (all on a C57BL/6 background) were obtained from Jackson Laboratory (Bar Harbor, ME) and *Nu/Nu* mice were obtained from Charles River Laboratory (Wilmington, MA). MMTV-PyMT mice (on C57BL/6 [referred to as BL/6] background) were bred at Cold Spring Harbor Laboratory (CSHL), and MMTV-PyMT-chOVA mice (Engelhardt et al., 2012) were a kind gift from Dr.

Mathew Krummel (University of California, San Francisco). MMTV-PyMT and PyMT-chOVA mice were intercrossed with *Ccr2*$^{-/-}$ mice. MMTV-PyMT;*Ccr2*$^{+/+}$ and MMTV-PyMT;*Ccr2*$^{-/-}$ mice, and similarly MMTV-PyMT-chOVA;*Ccr2*$^{+/+}$ and MMTV-PyMT-chOVA;*Ccr2*$^{-/-}$ mice, were from the same mouse colony (mice were littermates or their parents were littermates). All the BL/6 host mice were purchased from Jackson Lab. For primary tumor growth, mice were either sacrificed at end point- when tumors reached 20 mm or ulcerated (whichever came first)- or at indicated time points. Tumors were also collected either in the early growth phase (3 weeks after transplantation) or in the established growth-restricted phase for the *Ccr2*$^{-/-}$ tumors (5-6 weeks after transplantation). For lung metastasis assay, mice were sacrificed at either of two IACUC-approved endpoints- when tumors reached 25 mm or ulcerated. All animal experiments were approved by the Institutional Animal Care and Use Committee (IACUC) at CSHL and were conducted in accordance with the NIH Guide for the Care and Use of Laboratory Animals.

**Measurement of *in vivo* tumor growth and lung metastasis**

Tumor onset was determined by weekly palpation. Once a tumor was detected, its size was measured weekly by caliper, and tumor volume was calculated as (length x width$^2$)/2. Mice were sacrificed at either of two IACUC-approved endpoints: when tumors reached 25 mm or ulcerated. To determine metastatic burden, we adapted a previously published method (Nielsen et al., 2001). Briefly, lungs were placed in 4% paraformaldehyde (PFA) in phosphate-buffered saline (PBS) in a vacuum desiccator for 1 h. The lungs remained in 4% PFA at 4°C for 48 h, followed by incubation in 20% sucrose in PBS at 4°C for 48 h. Lungs were embedded in Tissue-Tek O.C.T. compound embedding solution (Sakura, Torrance, CA). The blocks were then placed in a custom-made cutting chamber with razor blade inserts every 2 mm, and the block was cut into 2 mm sections. These sectioned lung pieces were then re-embedded in fresh O.C.T. to allow for cross-sectional cuts from the entire lung tissue. These cross-sections of the lungs were stained

with H&E and scanned by an Aperio ScanScope® CS System (Leica Biosystems, Buffalo Grove, IL). The metastatic burden was calculated as the percentage of metastasis/lung area and the number of foci/lung area, determined using Aperio eSlide Capture Devices software (Leica Biosystems). Histology was evaluated by pathologist J.E.W. and scored as percentage solid areas of tumors.

**Primary cancer cell isolation, culture, and transplantation**

Aged-matched virgin females (C57BL/6, *Ccr2*$^{-/-}$, *Batf3*$^{-/-}$, or *Nu/Nu*), 6-12 weeks of age, were used as hosts for transplantation. Cancer cells were isolated from 2-3 tumors, each one 8-10 mm in diameter, from MMTV-PyMT;*Ccr2*$^{+/+}$ or MMTV-PyMT;*Ccr2*$^{-/-}$ mice. Tumors were mechanically dissociated and digested for 1 h with 1x collagenase/hyaluronidase (10X Solution, Stem Cell Technology, Cambridge, MA) containing DNase I (2 U/ml, Roche, Pleasanton, CA) in Roswell Park Memorial Institute (RPMI)-1640 medium supplemented with 5% FBS (VWR Life Science Seradigm, Philadelphia, PA). Single cells and debris were removed from the resulting carcinoma organoid preparation by pulse centrifugation in HBSS supplemented with 5% FBS. Purified carcinoma organoids were dissociated into single cell suspension in 0.05% trypsin with 0.1% EDTA supplemented with 2 U/ml of DNase I (Roche) for 2-3 min. Single tumor cells were passed through a 100 µm cell strainer (BD Biosciences, San Jose, CA) and either plated in RPMI-1640 supplemented with 10% FBS for *in vitro* experiments or washed with PBS and immediately injected into the fourth inguinal mammary fat pad of host mice ($2.5\times10^5$ in 20 µl of 1:1 PBS/Matrigel; Corning, Corning, NY).

To evaluate the effect of cancer cell *Ccr2* on the anti-tumor immune response locally vs. systemically, contralateral transplantation was conducted with cancer cells with different *Ccr2* genotype transplanted into each inguinal mammary fat pad ($2.5\times10^5$ in 20 µl of 1:1 PBS:Matrigel; Corning,

Corning, NY). Cancer cells were isolated as described above and both C57BL/6 and *Ccr2*$^{-/-}$ mice were used as hosts.

To transplant irradiated cancer cells, freshly isolated primary MMTV-PyMT;*Ccr2*$^{+/+}$ or MMTV-PyMT;*Ccr2*$^{-/-}$ cancer cells were plated in a 10 cm petri dish (2x10$^6$ per dish) in RPMI with 10% FBS, and received 80 Gy of irradiation in the Gammacell 40 Exactor (Best Theratronics, Ottawa, Ontario, Canada). After irradiation, cancer cells were washed with PBS and injected into the inguinal mammary fat pad of host mice (2.5×10$^5$ in 20 µl of PBS). To generate cancer cell conditioned medium, primary cancer cells from either MMTV-PyMT;*Ccr2*$^{+/+}$ or MMTV-PyMT;*Ccr2*$^{-/-}$ tumors were plated in a 10 cm dish (2x10$^6$ per dish) in DMEM/F12 medium plus 10% FBS, 1% penicillin/streptomycin, with or without CCR2 antagonist (RS504393, 10 µM, Sigma-Aldrich, St. Louis, MO) for two days. The conditioned medium was collected and centrifuged at 300 x g for 10 min, and the supernatant was used in experiments.

To determine surface MHC class I expression, primary cancer cells from MMTV-PyMT;*Ccr2*$^{+/+}$ tumors were plated in a 6-well plate (1x10$^6$ per well) in DMEM/F12 medium plus 10% FBS, 1% penicillin/streptomycin, with or without CCR2 antagonist (RS504393, 10 µM, Sigma-Aldrich) or recombinant mouse CCL2 (479-JE, 10 ng/ml, R&D Systems, Minneapolis, MN) for 24 or 48 h as indicated in the legend.

### *In vivo* antibody treatment

Tumor cells from MMTV-PyMT;*Ccr2*$^{+/+}$ or MMTV-PyMT;*Ccr2*$^{-/-}$ mice were transplanted as described above. For anti-PD-L1 treatment, on days 15, 18, 21, and 24 after transplantation, (after tumors had formed), mice received 200 µg of anti-PD-L1 antibody by intraperitoneal injection (Clone 10F.9G2; Bio X Cell, West Lebanon, NH) or control rat IgG2b antibody (Bio X Cell) (Winograd et al., 2015). For CD8+ T cell depletion, mice were injected intraperitoneally with 200 µg of anti-CD8a antibody (Clone 2.43;

BE0061; Bio X Cell, West Lebanon, NH) or control rat IgG2b antibody (Clone LTF-2; BE0090; Bio X Cell, West Lebanon, NH) every three days starting from day 0 until day 30. Tumor size was measured biweekly, and mice were sacrificed at IACUC-approved endpoint.

**Flow cytometry**

Tumors were harvested and mechanically dissociated for 30 min with Collagenase D (2 mg/ml; Sigma-Aldrich) and DNase I (4 U/ml; Roche) in RPMI. For flow cytometry of cells from lymph nodes, the lymph nodes were forced through a 100 μm cell strainer (BD Biosciences), and flow-through cells were collected for experiments. Cells were resuspended in 1x HBSS supplemented with 0.5% BSA and centrifuged at 300 x g. The cell suspension was filtered through a 70 μm cell strainer, and red blood cells were lysed using red blood cell lysing buffer (Sigma-Aldrich) for 1 min at room temperature.

For flow cytometry staining, cells ($1\times10^6$) were incubated with mouse Fc Block (clone 2.4G2, BD Biosciences) for 10 min on ice, and then were stained with the appropriate antibodies to surface markers at 4°C for 30 min in the dark or were permeabilized and stained with intracellular antibodies overnight (see below for antibodies). Cell viability stain Zombie Red (BioLegend, San Diego, CA) was used to differentiate between dead and live cells. The stained populations were analyzed using an LSR II flow cytometer (BD, Franklin Lakes, NJ) (see **Fig. S2** for gating strategies) and FlowJo software (BD, Version 10). Antibodies: CD45-eFluor 450 (Clone 30-F11), CD11c-PE-Cy7 (Clone N418), MHC II (I-A/I-E)-APC-eFlour780 (Clone M5/114.15.2), CD103-FITC (Clone 2E7), CD274 (B7-H1, PD-L1)-PE-Cy7 (Clone MIH5), CD3-FITC (Clone 17A2), CD8-eFluor450 (Clone 53-6.7), CD107a (LAMP-1)-PE (Clone 1D4B), IFN-γ-PE (Clone XMG1.2), Granzyme B-FITC (Clone NGZB), γδ TCR-PE-Cy5 (Clone GL3), and FoxP3-PE (Clone NRRF-30) all from eBioscience (Waltham, MA); CD4-PerCP-Cy5.5 (Clone BM9), CD69-PE (Clone H1.2F3), F4/80-PerCP-Cy5.5 (Clone BM9), MHC I (H-2)-PE (Clone M1/42), CD326

(EpCAM)-APC (Clone G8.8) and CD86-BV510 (Clone GL-1) all from BioLegend; CD45-APC (Clone 30-F11), Ly6G-FITC (Clone 1A8), and CD11b-PE (Clone M1/70) from BD Pharmingen; EpCAM-APC (Clone CI:A3-1, AbD Serotec [Hercules, CA]) and CCR2-flourescein (Clone 475301, R&D Systems). Prior to Granzyme B staining, cells were incubated for 2 h with Brefeldin A (Sigma-Aldrich, #B6542).

**Cytokine array**

Tumors (8-10 mm in diameter) were isolated from MMTV-PyMT;*Ccr2*$^{+/+}$ and MMTV-PyMT;*Ccr2*$^{-/-}$ mice and immediately snap-frozen in liquid nitrogen. They were then homogenized in PBS with the addition of protease inhibitors (Promega, Madison, WI). Proteome Profiler Mouse Cytokine Array Kit, Panel A (R&D Systems) was used according to the manufacturer's instructions. Films were scanned, and spots were analyzed using ImageJ software.

**MTS assay**

Proliferation of cancer cells isolated from MMTV-PyMT;*Ccr2*$^{+/+}$ and MMTV-PyMT;*Ccr2*$^{-/-}$ mice was measured using the CellTiter 96® AQueous One Solution Cell Proliferation Assay (MTS; Promega) according to the manufacturer's instructions. In this assay, the MTS tetrazolium compound (Owen's reagent) was bioreduced by metabolically active cells into a colored formazan product. The quantity of formazan product was measured in a 96-well plate by absorbance at 490 nm.

**RNA purification and real-time quantitative PCR (RT-qPCR) analysis**

Total RNA from cancer cells (cultured 48 hours in RPMI supplemented with 10% FBS) or primary tumors was extracted using an RNAeasy kit (Qiagen, Germantown, MD), following the manufacturer's instructions. RNA was quantified using a Nanodrop 2000 spectrophotometer (Thermo Fisher Scientific,

Waltham, MA). Reverse transcription was performed with an ImProm-II Reverse Transcription System (Promega) for the cancer cells, or the RevertAid First Strand cDNA Synthesis system (Thermo, K1622) for the primary tumors, with the following cycling conditions: 5 min at 70°C, 10 min at 4°C, 5 min at 25°C, 60 min at 42°C, and 15 sec at 70°C using 1 µg of total RNA extract for 20 µL of final volume. RT-qPCR analysis was performed using a TaqMan gene expression assay (Thermo Fisher Scientific) with the following specific primers: *Ccr2*: (Boring et al., 1997) and Mm00438270_m1; *Pd-l1:* Mm00452054_m1; *Cd8a*: Mm01182107_g1; *Ifn-g:* mm01168134_m1; *Pd-1*: mm01285676_m1; *Gzmb*: mm00502528_m1; *Ctla4*: mm00486849_m1; *Prf1*: mm00812512_m1; *Clec9a*: mm00554956_m1; *Cxcl9*: mm00434946_m1; *Cxcl10*: mm00445235_m1; *Cxcr3*: mm00438259_m1; *Cxcr4*: Mm01996749_s1; *Cd11c*: mm00498698_m1; *Cd40*: mm00441891_m1; *Cd80*: mm00711660_m1; *Cd86*: mm00444543_m1; *Ccl5*: mm01302427_m1; *Il-12b*: mm01288989_m1; *Tim3*: mm00454540_m1; *Csf2*: mm01290062_m1; *Flt3l*: mm00442801_m1; *Flt3*: mm00439016_m1; *Ccl2*: mm00441242_m1; *Csf3*: mm00438334_m1; *Csf1*: mm00432686_m1 and *Tbp*: mm01277042_m1.. For cancer cells, RT-qPCR was performed on three independently isolated cancer cell populations and in triplicate for each sample. For tumor samples, RT-qPCR was performed on at least five primary tumors from different mice, and in triplicate for each sample. Relative quantitation was performed with the $2^{(-\Delta\Delta CT)}$ method using *β-Actin* or *Tbp* expression for normalization and MMTV-PyMT;*Ccr2*$^{+/+}$ cancer cells or tumor samples as a reference sample.

**RNA *in situ* hybridization**

RNA *in situ* hybridization (ISH) was performed on PFA-fixed paraffin-embedded tissue sections using an RNAscope Chromogenic 2.0 Detection Kit (Advanced Cell Diagnostics [ACD], Inc., Newark, CA). A *Ccr2* probe was custom-designed by ACD, Inc. (Catalog number 436261-C2) and used according to the manufacturer's instructions. We confirmed that no signal was found with the probe using *Ccr2*$^{-/-}$ tissues.

Fluorescent RNA ISH for *Ccr2, Krt8, Cd8a,* and *Ifn-g* was performed on fresh frozen tissue sections using an RNAscope Fluorescent Multiplex Assay Kit (Advanced Cell Diagnostics [ACD], Inc., Newark, CA) with the following probes (by ACD): *Ccr2*: 436261-C2; *Krt18*: 424531-C1; *Cd8a*: 401681-C1; *Ifn-g*: 311391-C3) and used according to the manufacturer's instructions. For *Ccr2* FISH, we confirmed that no signal was found with the probe using *Ccr2*$^{-/-}$ tissues.

**Hematoxylin and eosin staining**

PFA-fixed paraffin-embedded tissue sections were deparaffinized and rehydrated following standard protocols, stained with Gill's Hematoxylin (Thermo Fisher Scientific, REF6765008) for 3 min, washed in tap water, rinsed with Nu-Clear II (Thermo Fisher Scientific, REF6769009), and then rinsed again first with tap water and then with Bluing Reagent (Thermo Fisher Scientific, REF 6769001). Slides were then stained with eosin (Sigma, HT110180), dehydrated following standard protocols, air-dried, and mounted with Cytoseal 60 (Thermo Fisher Scientific, Catalog number 831016).

**Immunofluorescence staining**

To stain for cytokeratin 5 and cytokeratin 8, paraffin sections were deparaffinized and rehydrated and antigen retrieval was carried out by boiling slides in Tris EDTA buffer (10 mM Tris Base, 1 mM EDTA, pH 9.0) for 6 min in a pressure cooker. The slides were blocked with 1x blocking buffer (PBS containing 2.5% BSA and 5% goat serum) and Fc receptor blocker (Innovex Biosciences), before incubating with anti-cytokeratin 5-Alexa Fluor 488 conjugated antibody (ab193894; 1:200 dilution; Abcam) and anti-Cytokeratin 8-Alexa Fluor 405 conjugated antibody (ab210139; 1:200 dilution; Abcam) overnight at 4°C. Sections were counterstained with ToPro-3 (1:1000 dilution; Life Technologies).

For all other stainings, frozen tissue sections were incubated with 1x blocking buffer (5% goat serum, 2.5% BSA in PBS) and Fc receptor blocker (Innovex Biosciences, Richmond, CA). Sections were incubated with rabbit anti-CD3 polyclonal antibody (1:500 dilution; Abcam, Cambridge, MA), rat anti-MHC class I monoclonal antibody (Clone ER-HR52, 1:100 dilution; Abcam), rat anti-PyMT antibody (Ab15085, 1:200; Abcam), rabbit anti-cleaved caspase-3 (Asp175) (D3E9) (#9579; 1:200 dilution; Cell Signaling Technology), anti-CD8a-Alexa Fluor 488 (Clone 5.3-6.7), anti-CD11c-Alexa Fluor 488 (Clone N418), or anti-CD326 (EpCAM)-APC (Clone G8.8) in 0.5x blocking buffer overnight at 4°C. Secondary antibodies (not used for primary antibodies conjugated to Alexa-Fluor 488) anti-rabbit-Alexa568, or anti-rat-Alexa568 (1:150 dilution; Life Technologies) were used for detection, and sections were counterstained with DAPI (1:200 dilution; Life Technologies). Images were collected at 40x magnification using a Leica SP8 confocal or an AX10 microscope and an AxioCam HRc camera (Zeiss, Thornwood, NY) and were analyzed using Volocity software (Version 6.3.0, PerkinElmer, Waltham, MA).

**Immunohistochemistry and terminal deoxynucleotidyl transferase dUTP nick end labeling (TUNEL) staining**

Sections were deparaffinized and rehydrated for phospho-STAT3 and Ki67 staining. Antigen retrieval was carried out by boiling slides in 10 mM sodium citrate buffer (pH 6.0) for 6 min in a pressure cooker, while for phospho-STAT1 staining, antigen retrieval was done in Tris EDTA buffer (10 mM Tris Base, 1 mM EDTA, pH 9.0). The slides were blocked with 3% hydrogen peroxide, 1x blocking buffer (PBS containing 2.5% BSA and 5% goat serum), Fc receptor blocker (Innovex Biosciences), and finally avidin/biotin blocking buffer (Vector Laboratories, Burlingame, CA, SP-2001). Slides were then incubated with primary antibodies overnight at 4°C in 0.5x blocking buffer: rabbit anti-Ki67/MK167

(1:1,000 dilution; Novus International, Saint Charles, MO, NB110-89717), rabbit anti-phospho-STAT1 (1:200 dilution; Cell Signaling Technology, Danvers, MA), or rabbit anti-phospho-STAT3 (1:500 dilution; Cell Signaling Technology). After incubating with secondary biotinylated goat anti-rabbit IgG antibody (1:500, Vector Laboratories, BA-1000) for 1 h at room temperature, slides were incubated with avidin-conjugated horseradish peroxidase (Vector Laboratories, PK-6100) for 30 min, and the signals were detected by a DAB (3,3'-Diaminobenzidine) substrate kit (Vector Laboratories, SK-4100). Lastly, sections were counter-stained with hematoxylin. TUNEL staining was performed on deparaffinized sections to detect late-stage apoptotic cells using the ApopTag peroxidase *in situ* apoptosis detection kit (Millipore, Burlington, MA), according to the manufacturer's instructions. Images were scanned by an Aperio ScanScope® CS System (Leica Biosystems), and positive nuclei were counted using Aperio eSlide Capture Devices software (Leica Biosystems).

**ImmunoSEQ**

Tumors from *Ccr2*$^{+/+}$ and *Ccr2*$^{-/-}$ transplants were isolated and immediately placed in liquid nitrogen for shipment. Amplification and sequencing were performed on the immunoSEQ platform (Adaptive Biotechnologies, Seattle, WA) using a multiplex PCR-based assay that exclusively targets rearranged T cell receptor genes. Sequencing data were analyzed using immunoSEQ Analyzer software. Shannon's Entropy (H), a measure of the richness and uniformity of the frequency of the T cell receptor repertoire distribution, was defined as:

$$H = -\sum_{i=1}^{N} P_i \log_2 P_i$$

Where N equals the number of unique clones and $P_i$ the frequency of clones. To account for variation in sequencing depth, entropy was normalized by its maximum value ($H_{max}$):

$$H_N = H / H_{max}$$

Clonality is defined as C = 1 - $H_N$. (Sherwood et al., 2013). Sequencing files are available from the Adaptive Biotechnologies immunoSEQ web site.

**Transcriptional profiling and bioinformatics analysis**

*Ccr2*$^{+/+}$ or *Ccr2*$^{-/-}$ cancer cells were isolated from tumors and sorted as EpCAM+CD45-CD31- live cells (using 7-AAD Viability Staining Solution, Thermo Fisher Scientific) four weeks after orthotopic transplantation into the mammary fat pad of wild-type C57BL/6 mice. Total cancer cell RNA was extracted using a TRIzol extraction protocol. cDNA libraries were prepared using the Ovation® RNA-Seq System V2 (NuGEN Technologies, San Carlos, CA) according to the manufacturer's protocol and sequenced using a NextSeq 500 instrument (Illumina, San Diego, CA) to obtain 388 million 76 bp single-end reads. Reads were mapped to the reference mm9 mouse genome using Spliced Transcripts Alignment to a Reference (STAR) (Dobin et al., 2013) and were determined using HTSeq (Anders et al., 2015). Differential gene expression analysis was performed using DESeq2 (Love et al., 2014) with a false discovery rate cutoff of 5%. Hierarchical clustering was performed by sample and gene using normalized and log2-transformed gene expression values of differentially expressed genes. All of the analyses described above were performed on the Bioinformatics Shared Resource Galaxy server at CSHL. Gene set enrichment analysis (Subramanian et al., 2005) was performed on a pre-ranked gene list sorted by log2FoldChange value against v5.1 Hallmark gene sets using default parameters. Gene ontology term enrichment analysis was performed using GOrilla PANTHER (Eden et al., 2009).

**Bone marrow-derived dendritic cell (BMDC) isolation, culture, and activation**

BMDCs were Isolation and cultured as previously described (Inaba et al., 1992). Briefly, bone marrow was obtained from female C57BL/6 mice by flushing the femur and tibia with 2 ml of HBSS using a 1 ml insulin syringe with a 29G × ½ needle. The cells were washed with HBSS twice by centrifugation at 250 x g for 8 min and then suspended in BMDC culture medium (RPMI-1640 medium [Thermo Fisher Scientific] containing 10% FBS, 20 ng/ml recombinant mouse GM-CSF [BioLegend], 50 units/ml penicillin, and 50 μg/ml streptomycin). The cells were then plated in 10 cm culture plates ($2\times10^6$ cells per petri dish) and kept at 37°C in a 5% $CO_2$ incubator for three days, then split at day 4 into two plates. For activation of BMDCs with cancer cell conditioned medium, the non-attached BMDCs were harvested at day 6 by gently pipetting the cultures with medium. This BMDC population was then rinsed three times in HBSS and suspended in a) culture medium, b) conditioned medium from either MMTV-PyMT;*Ccr2*$^{-/-}$ or MMTV-PyMT;*Ccr2*$^{+/+}$ cancer cells, or c) conditioned medium from MMTV-PyMT;*Ccr2*$^{+/+}$ cancer cells cultured with CCR2 antagonist (RS504393, 10 μM, Sigma-Aldrich). After incubation with conditioned medium for 24 h, non-adherent BMDCs were harvested for flow cytometry.

**Chromium release assay**

Cytotoxic CD8+ T cells were isolated from spleens of OT-I transgenic mice by magnetic labeling and separation (Miltenyi Biotec, Cambridge, MA). Briefly, the spleen was forced through a 100 μm cell strainer (BD Biosciences), and flow-through cells were collected. After lysing red blood cells, the splenocytes were washed and incubated with CD8a+ T Cell Biotin-Antibody Cocktail, mouse (Miltenyi Biotec) at 4°C for 5 min, followed by incubating with anti-Biotin microbeads (Miltenyi Biotec) at 4°C for 10 min. The cell suspension was applied to an LS column (Miltenyi Biotec) in a magnetic field, and the flow-through (negatively selected) CD8+ T cells were collected. The isolated CD8+ T cells were cultured on plates coated with anti-mouse-CD3 (BioLegend) in RPMI-1640 containing 10% FBS, 50 μM of β-

mercaptoethanol, 20 ng/ml mouse IL-2, 2 ng/ml mouse IL-7, and 1% penicillin/streptomycin for 6-9 days. Primary cancer cells were isolated as described above from MMTV-PyMT-chOVA;*Ccr2*$^{+/+}$ or MMTV-PyMT-chOVA;*Ccr2*$^{-/-}$ mice and cultured overnight with or without CCR2 antagonist (10 μM, Sigma RS504393) and OVA peptides (1 μg/ml) in DMEM/F12 medium with 10% FBS. The E0771 cancer cell line was infected with lentivirus expressing luciferase and eGFP fusion and fused OVA SIINFEKL peptide to the C-terminus to eGFP. Transduced cells were sorted by flow cytometry for eGFP positive cells. For chromium ($^{51}$Cr) release assay, cancer cells (1,000 per well) were incubated with 50 μl of $^{51}$Cr solution (activity 1 mCi/ml, PerkinElmer) plus 50 μl of RPMI medium with 10% FBS for 2 h at 37°C. After rinsing the cells three times with RPMI plus 10% FBS, 50 μl of cancer cells (1,000) were plated into each well of a 96-well, V-bottom plate, followed by the addition of 50 μl of CD8+ T cells at a ratio of 10:1. After 4 h of incubation at 37°C, 50 μl of supernatant from each well was transferred to miniature vials, and radioactivity was determined by a Beckman scintillation counter (PerkinElmer). The percentage of specific lysis was calculated using the standard formula [(experimental - spontaneous release)/(total - spontaneous release) x 100] and expressed as the mean of triplicate samples.

**Western blot**

Snap-frozen tumor samples were homogenized in radio immunoprecipitation assay buffer with cOmplete™ Protease Inhibitor Cocktail Tablets (Roche) and phosphatase inhibitor cocktail (Thermo Fisher Scientific), and lysis was performed on ice for 30 min. Cell lysates were centrifuged for 15 min at 12,000 x g at 4°C. After centrifugation, the supernatant was mixed with 4x loading buffer plus 2.5% of β-mercaptoethanol and loaded on 8% SDS/PAGE gels. Protein bands were transferred to PVDF membranes (Bio-RAD) at 90 V for 2 h in a Bio-Rad Mini Trans-Blot system. The membrane was incubated sequentially with different primary antibodies: anti-p65, anti-p-p65, anti-p-STAT1, anti-p-STAT3, and

anti-STAT3 (all from Cell Signaling Technology), and anti-STAT1 and anti-beta-Actin (from Santa Cruz Biotechnology, Dallas, Tx). Secondary antibodies were from LI-COR, (Lincoln, NE). Protein detection was performed using the Odyssey imaging system (LI-COR).

**ELISA**

Conditioned medium from *Ccr2*$^{+/+}$ and *Ccr2*$^{-/-}$ cancer cells was collected, and GM-CSF concentration was evaluated by ELISA, following the manufacturer's instructions (R&D Systems). Briefly, 50 µl of cytokine standard or conditioned medium was added to the wells of the pre-coated ELISA plate and incubated at room temperature for 2 h. Plates were washed five times with wash buffer and incubated with a horseradish peroxidase-linked polyclonal antibody specific to mouse GM-CSF for 2 h, followed by incubation with substrate solution for 30 min. After adding 100 µL of stop solution, the optical density of each well was measured at 450 nm using a microplate reader. The concentrations of GM-CSF in the conditioned medium were calculated according to the standard curve.

**Whole mount carmine staining of mammary glands**

Mammary glands were isolated and spread on glass slides, exposing as much area as possible. Then, the mammary glands were fixed in Carnoy's Fixative (60% ethanol, 30% chloroform and 10% glacial acetic acid) for 2-4 hours at room temperature, followed by 15 minute washes in 70% and 50% ethanol, respectively, with a final rinse in double-distilled water. The glands were then stained with carmine red stain (2.5 g aluminum potassium sulfate, 1 g carmine, and $dH_2O$ to a final volume of 500 mL, boiled for 25 minutes) for 16 hours or until the fat pad was a uniform pink color. After staining, the mammary glands were de-stained in 1% solution of 1N HCl in 70% ethanol. De-stained glands were rinsed twice for 15

minutes in 70% ethanol followed by 15-minute washes in 90% and 100% ethanol, respectively. The mammary glands were then placed in xylene for 2 hours for clearing and then mounted.

**Statistical analysis**

All statistical analyses were performed using GraphPad Prism Version 6 software. Data were analyzed using Kaplan-Meier survival analysis, Student's t-tests, ANOVA, two-way ANOVA, chi-Square test, and log-rank (Mantel-Cox) test, as indicated in the figure legends, with an alpha of 0.05. The number of sampled units, N, is indicated in the figure legends.

**ACKNOWLEDGEMENTS**

We thank Kristina Grigaitytė for assistance with TCGA patient RNA-seq data analysis and Laura Maiorino for drawing the included illustrations. This work was supported by funds from the CSHL Cancer Center (P30-CA045508) and the Department of Defense (W81XWH-14-1-0078) to M.E.; from the Charles and Marie Robertson Foundation to X.Y.H.; from the Lustgarten Foundation, the National Cancer Institute, and the Cedar Hill Foundation to D.T.F.; from the Rita Allen Foundation and the V Foundation for Cancer Research to C.O.d.S.; a Starr Centennial Scholarship from the Watson School of Biological Sciences to E.B; and R.Y is a George A. and Marjorie H. Anderson Fellow. Support was also provided by the State of New York (Contract #C150158), and the opinions, results, findings and/or interpretations of data contained therein do not necessarily represent the opinions, interpretations or policy of the State. **Competing interests:** D.T.F. is a co-founder of Myosotis, LLC, and a scientific advisory board member of iTeos Therapeutics, IFM Therapeutics, LLC, and Kymab. The other authors disclose no potential conflicts of interest.

## AUTHOR CONTRIBUTIONS

M.R.F. and M.E. designed the experiments. M.R.F. and X.Y.H. performed the *in vitro* experiments; M.R.F., C.O.d.S., and E.B. isolated RNA from cancer cells and performed the RNA-seq analysis. M.R.F. and X.Y.H. performed the animal experiments; A.S.A., M.R.F., A.P., and X.Y.H. performed flow cytometry; J.E.W. analyzed the histological sections; and M.R.F., X.Y.H, and A.E. performed immunohistochemistry and *in situ* hybridizations. X.Y.H., A.P., R.Y., and M.R.F. designed and performed the chromium release experiments; and A.E., M.R.F., and X.Y.H. performed qPCR. L.V.A. and D.T.F. provided experimental advice. M.R.F., X.Y.H., and M.E. wrote the manuscript.

## Abbreviations

BMDC: bone marrow-derived dendritic cells

CCL2: C-C chemokine ligand 2

CCR2: C-C chemokine receptor type 2

chOVA: mCherry-ovalbumin

CTL: cytotoxic T lymphocyte

DC: dendritic cell

dLN: draining lymph node

G-CSF granulocyte colony-stimulating factor

GM-CSF: granulocyte-macrophage colony-stimulating factor

IACUC: Institutional Animal Care and Use Committee

IFN-γ: interferon gamma

LAMP-1: lysosomal-associated membrane protein 1

MDSC: myeloid-derived suppressor cell

MHC: major histocompatibility complex

MMTV: mouse mammary tumor virus

PD-L1: programmed cell death ligand 1

PFA: paraformaldehyde

PyMT: polyoma middle T

RPKM: reads per kilobase million

RPMI: Roswell Park Memorial Institute

TCGA: The Cancer Genome Atlas

TCR: T cell receptor

TUNEL: terminal deoxynucleotidyl transferase dUTP nick end labeling

**REFERENCES**

Ahn, R., V. Sabourin, A.M. Bolt, S. Hebert, S. Totten, N. De Jay, M.C. Festa, Y.K. Young, Y.K. Im, T. Pawson, A.E. Koromilas, W.J. Muller, K.K. Mann, C.L. Kleinman, and J. Ursini-Siegel. 2017. The Shc1 adaptor simultaneously balances Stat1 and Stat3 activity to promote breast cancer immune suppression. *Nat Commun* 8:14638.

Anders, S., P.T. Pyl, and W. Huber. 2015. HTSeq--a Python framework to work with high-throughput sequencing data. *Bioinformatics* 31:166-169.

Bayne, L.J., G.L. Beatty, N. Jhala, C.E. Clark, A.D. Rhim, B.Z. Stanger, and R.H. Vonderheide. 2012. Tumor-derived granulocyte-macrophage colony-stimulating factor regulates myeloid inflammation and T cell immunity in pancreatic cancer. *Cancer Cell* 21:822-835.

Bonapace, L., M.M. Coissieux, J. Wyckoff, K.D. Mertz, Z. Varga, T. Junt, and M. Bentires-Alj. 2014. Cessation of CCL2 inhibition accelerates breast cancer metastasis by promoting angiogenesis. *Nature* 515:130-133.

Boring, L., J. Gosling, S.W. Chensue, S.L. Kunkel, R.V. Farese, Jr., H.E. Broxmeyer, and I.F. Charo. 1997. Impaired monocyte migration and reduced type 1 (Th1) cytokine responses in C-C chemokine receptor 2 knockout mice. *J Clin Invest* 100:2552-2561.

Broz, M.L., M. Binnewies, B. Boldajipour, A.E. Nelson, J.L. Pollack, D.J. Erle, A. Barczak, M.D. Rosenblum, A. Daud, D.L. Barber, S. Amigorena, L.J. Van't Veer, A.I. Sperling, D.M. Wolf, and M.F. Krummel. 2014. Dissecting the tumor myeloid compartment reveals rare activating antigen-presenting cells critical for T cell immunity. *Cancer Cell* 26:638-652.

Chen, J., C.C. Jiang, L. Jin, and X.D. Zhang. 2016a. Regulation of PD-L1: a novel role of pro-survival signalling in cancer. *Ann Oncol* 27:409-416.

Chen, W., Q. Gao, S. Han, F. Pan, and W. Fan. 2015. The CCL2/CCR2 axis enhances IL-6-induced epithelial-mesenchymal transition by cooperatively activating STAT3-Twist signaling. *Tumour biology : the journal of the International Society for Oncodevelopmental Biology and Medicine* 36:973-981.

Chen, X., Y. Wang, D. Nelson, S. Tian, E. Mulvey, B. Patel, I. Conti, J. Jaen, and B.J. Rollins. 2016b. CCL2/CCR2 Regulates the Tumor Microenvironment in HER-2/neu-Driven Mammary Carcinomas in Mice. *PLoS One* 11:e0165595.

de Mingo Pulido, A., A. Gardner, S. Hiebler, H. Soliman, H.S. Rugo, M.F. Krummel, L.M. Coussens, and B. Ruffell. 2018. TIM-3 Regulates CD103(+) Dendritic Cell Function and Response to Chemotherapy in Breast Cancer. *Cancer Cell* 33:60-74 e66.

Deshmane, S.L., S. Kremlev, S. Amini, and B.E. Sawaya. 2009. Monocyte chemoattractant protein-1 (MCP-1): an overview. *Journal of interferon & cytokine research : the official journal of the International Society for Interferon and Cytokine Research* 29:313-326.

Dobin, A., C.A. Davis, F. Schlesinger, J. Drenkow, C. Zaleski, S. Jha, P. Batut, M. Chaisson, and T.R. Gingeras. 2013. STAR: ultrafast universal RNA-seq aligner. *Bioinformatics* 29:15-21.

Dunn, G.P., A.T. Bruce, H. Ikeda, L.J. Old, and R.D. Schreiber. 2002. Cancer immunoediting: from immunosurveillance to tumor escape. *Nat Immunol* 3:991-998.

Dunn, G.P., L.J. Old, and R.D. Schreiber. 2004. The three Es of cancer immunoediting. *Annu Rev Immunol* 22:329-360.

Eden, E., R. Navon, I. Steinfeld, D. Lipson, and Z. Yakhini. 2009. GOrilla: a tool for discovery and visualization of enriched GO terms in ranked gene lists. *BMC bioinformatics* 10:48.

Engelhardt, J.J., B. Boldajipour, P. Beemiller, P. Pandurangi, C. Sorensen, Z. Werb, M. Egeblad, and M.F. Krummel. 2012. Marginating dendritic cells of the tumor microenvironment cross-present tumor antigens and stably engage tumor-specific T cells. *Cancer Cell* 21:402-417.

Fang, W.B., I. Jokar, A. Zou, D. Lambert, P. Dendukuri, and N. Cheng. 2012. CCL2/CCR2 chemokine signaling coordinates survival and motility of breast cancer cells through Smad3 protein- and p42/44 mitogen-activated protein kinase (MAPK)-dependent mechanisms. *J Biol Chem* 287:36593-36608.

Freeman, G.J., A.J. Long, Y. Iwai, K. Bourque, T. Chernova, H. Nishimura, L.J. Fitz, N. Malenkovich, T. Okazaki, M.C. Byrne, H.F. Horton, L. Fouser, L. Carter, V. Ling, M.R. Bowman, B.M. Carreno, M. Collins, C.R. Wood, and T. Honjo. 2000. Engagement of the PD-1 immunoinhibitory receptor by a novel B7 family member leads to negative regulation of lymphocyte activation. *J Exp Med* 192:1027-1034.

Garrido, F., I. Romero, N. Aptsiauri, and A.M. Garcia-Lora. 2016. Generation of MHC class I diversity in primary tumors and selection of the malignant phenotype. *International journal of cancer* 138:271-280.

Greter, M., J. Helft, A. Chow, D. Hashimoto, A. Mortha, J. Agudo-Cantero, M. Bogunovic, E.L. Gautier, J. Miller, M. Leboeuf, G. Lu, C. Aloman, B.D. Brown, J.W. Pollard, H. Xiong, G.J. Randolph, J.E. Chipuk, P.S. Frenette, and M. Merad. 2012. GM-CSF controls nonlymphoid tissue dendritic cell homeostasis but is dispensable for the differentiation of inflammatory dendritic cells. *Immunity* 36:1031-1046.

Guy, C.T., R.D. Cardiff, and W.J. Muller. 1992. Induction of mammary tumors by expression of polyomavirus middle T oncogene: a transgenic mouse model for metastatic disease. *Molecular and cellular biology* 12:954-961.

Hildner, K., B.T. Edelson, W.E. Purtha, M. Diamond, H. Matsushita, M. Kohyama, B. Calderon, B.U. Schraml, E.R. Unanue, M.S. Diamond, R.D. Schreiber, T.L. Murphy, and K.M. Murphy. 2008. Batf3 deficiency reveals a critical role for CD8alpha+ dendritic cells in cytotoxic T cell immunity. *Science* 322:1097-1100.

Hu, Q., M. Myers, W. Fang, M. Yao, G. Brummer, J. Hawj, C. Smart, C. Berkland, and N. Cheng. 2019. Role of ALDH1A1 and HTRA2 expression in CCL2/CCR2-mediated breast cancer cell growth and invasion. *Biology open* 8:

Igney, F.H., and P.H. Krammer. 2002. Immune escape of tumors: apoptosis resistance and tumor counterattack. *J Leukoc Biol* 71:907-920.

Inaba, K., M. Inaba, N. Romani, H. Aya, M. Deguchi, S. Ikehara, S. Muramatsu, and R.M. Steinman. 1992. Generation of large numbers of dendritic cells from mouse bone marrow cultures supplemented with granulocyte/macrophage colony-stimulating factor. *J Exp Med* 176:1693-1702.

Izumi, K., L.Y. Fang, A. Mizokami, M. Namiki, L. Li, W.J. Lin, and C. Chang. 2013. Targeting the androgen receptor with siRNA promotes prostate cancer metastasis through enhanced macrophage recruitment via CCL2/CCR2-induced STAT3 activation. *EMBO molecular medicine* 5:1383-1401.

Jones, L.M., M.L. Broz, J.J. Ranger, J. Ozcelik, R. Ahn, D. Zuo, J. Ursini-Siegel, M.T. Hallett, M. Krummel, and W.J. Muller. 2016. STAT3 Establishes an Immunosuppressive Microenvironment during the Early Stages of Breast Carcinogenesis to Promote Tumor Growth and Metastasis. *Cancer Res* 76:1416-1428.

Labovsky, V., L.M. Martinez, K.M. Davies, M. de Lujan Calcagno, H. Garcia-Rivello, A. Wernicke, L. Feldman, A. Matas, M.B. Giorello, F.R. Borzone, H. Choi, S.C. Howard, and N.A. Chasseing. 2017. Prognostic significance of TRAIL-R3 and CCR-2 expression in tumor epithelial cells of patients with early breast cancer. *BMC cancer* 17:280.

Lebrecht, A., C. Grimm, T. Lantzsch, E. Ludwig, L. Hefler, E. Ulbrich, and H. Koelbl. 2004. Monocyte chemoattractant protein-1 serum levels in patients with breast cancer. *Tumour biology : the journal of the International Society for Oncodevelopmental Biology and Medicine* 25:14-17.

Lebrecht, A., L. Hefler, C. Tempfer, and H. Koelbl. 2001. Serum cytokine concentrations in patients with cervical cancer: interleukin-4, interferon-gamma, and monocyte chemoattractant protein-1. *Gynecologic oncology* 83:170-171.

Li, M., D.A. Knight, A.S. L, M.J. Smyth, and T.J. Stewart. 2013. A role for CCL2 in both tumor progression and immunosurveillance. *Oncoimmunology* 2:e25474.

Lim, S.Y., A.E. Yuzhalin, A.N. Gordon-Weeks, and R.J. Muschel. 2016. Targeting the CCL2-CCR2 signaling axis in cancer metastasis. *Oncotarget*

Lin, E.Y., J.G. Jones, P. Li, L. Zhu, K.D. Whitney, W.J. Muller, and J.W. Pollard. 2003. Progression to malignancy in the polyoma middle T oncoprotein mouse breast cancer model provides a reliable model for human diseases. *Am J Pathol* 163:2113-2126.

Love, M.I., W. Huber, and S. Anders. 2014. Moderated estimation of fold change and dispersion for RNA-seq data with DESeq2. *Genome Biol* 15:550.

Lu, Y., Z. Cai, D.L. Galson, G. Xiao, Y. Liu, D.E. George, M.F. Melhem, Z. Yao, and J. Zhang. 2006. Monocyte chemotactic protein-1 (MCP-1) acts as a paracrine and autocrine factor for prostate cancer growth and invasion. *The Prostate* 66:1311-1318.

Mayer, C.T., P. Ghorbani, A. Nandan, M. Dudek, C. Arnold-Schrauf, C. Hesse, L. Berod, P. Stuve, F. Puttur, M. Merad, and T. Sparwasser. 2014. Selective and efficient generation of functional Batf3-dependent CD103+ dendritic cells from mouse bone marrow. *Blood* 124:3081-3091.

Mehta, H.M., M. Malandra, and S.J. Corey. 2015. G-CSF and GM-CSF in Neutropenia. *J Immunol* 195:1341-1349.

Meyer, M.A., J.M. Baer, B.L. Knolhoff, T.M. Nywening, R.Z. Panni, X. Su, K.N. Weilbaecher, W.G. Hawkins, C. Ma, R.C. Fields, D.C. Linehan, G.A. Challen, R. Faccio, R.L. Aft, and D.G. DeNardo. 2018. Breast and pancreatic cancer interrupt IRF8-dependent dendritic cell development to overcome immune surveillance. *Nat Commun* 9:1250.

Mitchell, L.A., R.J. Hansen, A.J. Beaupre, D.L. Gustafson, and S.W. Dow. 2013. Optimized dosing of a CCR2 antagonist for amplification of vaccine immunity. *International immunopharmacology* 15:357-363.

Muller, A., B. Homey, H. Soto, N. Ge, D. Catron, M.E. Buchanan, T. McClanahan, E. Murphy, W. Yuan, S.N. Wagner, J.L. Barrera, A. Mohar, E. Verastegui, and A. Zlotnik. 2001. Involvement of chemokine receptors in breast cancer metastasis. *Nature* 410:50-56.

Nakasone, E.S., H.A. Askautrud, T. Kees, J.H. Park, V. Plaks, A.J. Ewald, M. Fein, M.G. Rasch, Y.X. Tan, J. Qiu, J. Park, P. Sinha, M.J. Bissell, E. Frengen, Z. Werb, and M. Egeblad. 2012. Imaging tumor-stroma interactions during chemotherapy reveals contributions of the microenvironment to resistance. *Cancer Cell* 21:488-503.

Nielsen, B.S., L.R. Lund, I.J. Christensen, M. Johnsen, P.A. Usher, L. Wulf-Andersen, T.L. Frandsen, K. Dano, and H.J. Gundersen. 2001. A precise and efficient stereological method for determining murine lung metastasis volumes. *The American journal of pathology* 158:1997-2003.

Nywening, T.M., A. Wang-Gillam, D.E. Sanford, B.A. Belt, R.Z. Panni, B.M. Cusworth, A.T. Toriola, R.K. Nieman, L.A. Worley, M. Yano, K.J. Fowler, A.C. Lockhart, R. Suresh, B.R. Tan, K.H. Lim, R.C. Fields, S.M. Strasberg, W.G. Hawkins, D.G. DeNardo, S.P. Goedegebuure, and D.C. Linehan. 2016. Targeting tumour-associated macrophages with CCR2 inhibition in combination with FOLFIRINOX in

patients with borderline resectable and locally advanced pancreatic cancer: a single-centre, open-label, dose-finding, non-randomised, phase 1b trial. *The lancet oncology* 17:651-662.

Pylayeva-Gupta, Y., K.E. Lee, C.H. Hajdu, G. Miller, and D. Bar-Sagi. 2012. Oncogenic Kras-induced GM-CSF production promotes the development of pancreatic neoplasia. *Cancer Cell* 21:836-847.

Qian, B., Y. Deng, J.H. Im, R.J. Muschel, Y. Zou, J. Li, R.A. Lang, and J.W. Pollard. 2009. A distinct macrophage population mediates metastatic breast cancer cell extravasation, establishment and growth. *PLoS One* 4:e6562.

Qian, B.Z., J. Li, H. Zhang, T. Kitamura, J. Zhang, L.R. Campion, E.A. Kaiser, L.A. Snyder, and J.W. Pollard. 2011. CCL2 recruits inflammatory monocytes to facilitate breast-tumour metastasis. *Nature* 475:222-225.

Roberts, E.W., M.L. Broz, M. Binnewies, M.B. Headley, A.E. Nelson, D.M. Wolf, T. Kaisho, D. Bogunovic, N. Bhardwaj, and M.F. Krummel. 2016. Critical Role for CD103(+)/CD141(+) Dendritic Cells Bearing CCR7 for Tumor Antigen Trafficking and Priming of T Cell Immunity in Melanoma. *Cancer Cell* 30:324-336.

Rodriguez-Frade, J.M., A.J. Vila-Coro, A.M. de Ana, J.P. Albar, A.C. Martinez, and M. Mellado. 1999. The chemokine monocyte chemoattractant protein-1 induces functional responses through dimerization of its receptor CCR2. *Proc Natl Acad Sci U S A* 96:3628-3633.

Ruffell, B., D. Chang-Strachan, V. Chan, A. Rosenbusch, C.M. Ho, N. Pryer, D. Daniel, E.S. Hwang, H.S. Rugo, and L.M. Coussens. 2014. Macrophage IL-10 blocks CD8+ T cell-dependent responses to chemotherapy by suppressing IL-12 expression in intratumoral dendritic cells. *Cancer Cell* 26:623-637.

Sherwood, A.M., R.O. Emerson, D. Scherer, N. Habermann, K. Buck, J. Staffa, C. Desmarais, N. Halama, D. Jaeger, P. Schirmacher, E. Herpel, M. Kloor, A. Ulrich, M. Schneider, C.M. Ulrich, and H. Robins. 2013. Tumor-infiltrating lymphocytes in colorectal tumors display a diversity of T cell receptor sequences that differ from the T cells in adjacent mucosal tissue. *Cancer immunology, immunotherapy : CII* 62:1453-1461.

Soria, G., and A. Ben-Baruch. 2008. The inflammatory chemokines CCL2 and CCL5 in breast cancer. *Cancer letters* 267:271-285.

Spranger, S., D. Dai, B. Horton, and T.F. Gajewski. 2017. Tumor-Residing Batf3 Dendritic Cells Are Required for Effector T Cell Trafficking and Adoptive T Cell Therapy. *Cancer Cell* 31:711-723 e714.

Subramanian, A., P. Tamayo, V.K. Mootha, S. Mukherjee, B.L. Ebert, M.A. Gillette, A. Paulovich, S.L. Pomeroy, T.R. Golub, E.S. Lander, and J.P. Mesirov. 2005. Gene set enrichment analysis: a knowledge-based approach for interpreting genome-wide expression profiles. *Proc Natl Acad Sci U S A* 102:15545-15550.

Winograd, R., K.T. Byrne, R.A. Evans, P.M. Odorizzi, A.R. Meyer, D.L. Bajor, C. Clendenin, B.Z. Stanger, E.E. Furth, E.J. Wherry, and R.H. Vonderheide. 2015. Induction of T-cell Immunity Overcomes Complete Resistance to PD-1 and CTLA-4 Blockade and Improves Survival in Pancreatic Carcinoma. *Cancer Immunol Res* 3:399-411.

Wolf, M.J., A. Hoos, J. Bauer, S. Boettcher, M. Knust, A. Weber, N. Simonavicius, C. Schneider, M. Lang, M. Sturzl, R.S. Croner, A. Konrad, M.G. Manz, H. Moch, A. Aguzzi, G. van Loo, M. Pasparakis, M. Prinz, L. Borsig, and M. Heikenwalder. 2012. Endothelial CCR2 Signaling Induced by Colon Carcinoma Cells Enables Extravasation via the JAK2-Stat5 and p38MAPK Pathway. *Cancer Cell* 22:91-105.

## FIGURE LEGENDS

### Fig. 1: Cancer cell CCR2 promotes primary tumor growth, reducing overall survival

**a.** Tumor onset (tumor-free survival) is similar for MMTV-PyMT;*Ccr2*$^{+/+}$, MMTV-PyMT;*Ccr2*$^{+/-}$, and MMTV-PyMT;*Ccr2*$^{-/-}$ mice, as determined by weekly palpation and caliper measurement. N.S.=non-significant (Log-rank [Mantel-Cox] test; n=28 MMTV-PyMT;*Ccr2*$^{+/+}$, 20 MMTV-PyMT;*Ccr2*$^{+/-}$, and 18 MMTV-PyMT;*Ccr2*$^{-/-}$ mice).

**b.** Primary tumor growth is reduced in MMTV-PyMT;*Ccr2*$^{+/-}$ and MMTV-PyMT;*Ccr2*$^{-/-}$ mice compared to MMTV-PyMT;*Ccr2*$^{+/+}$ mice, as determined by weekly caliper measurement (mean +/- SEM, two-way ANOVA; n=21 MMTV-PyMT;*Ccr2*$^{+/+}$, 25 MMTV-PyMT;*Ccr2*$^{+/-}$, and 18 MMTV-PyMT;*Ccr2*$^{-/-}$ mice).

**c.** Time until IACUC-approved endpoint was increased for MMTV-PyMT;*Ccr2*$^{+/-}$ and MMTV-PyMT;*Ccr2*$^{-/-}$ mice compared to MMTV-PyMT;*Ccr2*$^{+/+}$ mice (Log-rank [Mantel-Cox] test; n=30 MMTV-PyMT;*Ccr2*$^{+/+}$, 35 MMTV-PyMT;*Ccr2*$^{+/-}$, and 29 MMTV-PyMT;*Ccr2*$^{-/-}$ mice).

**d.** Cancer cells express CCR2 (arrows) as determined by RNA *in situ* hybridization for *Ccr2* performed on paraffin-embedded tumor sections from MMTV-PyMT;*Ccr2*$^{+/+}$ mice. Image is representative of more than 10 mice. Scale bar=20 μm.

**e.** CCR2 is highly expressed on epithelial cells, as determined by flow cytometry performed on *Ccr2*$^{+/+}$ or *Ccr2*$^{-/-}$ tumors transplanted to C57BL/6 hosts. Anti-CCR2 primary antibody was gated on EpCAM+ cells and compared to background levels. Left panel shows one representative experiment and right panel depicts median fluorescence intensity for all experiments (mean +/- SEM, Student's t-test; n=5).

**f.** Schematic of transplantation experiments.

**g.** Primary tumor growth of *Ccr2*$^{-/-}$ cancer cells is reduced compared to that of *Ccr2*$^{+/+}$ cancer cells regardless of the genotype of the host, as determined by weekly caliper measurement (mean +/- SEM, two-way ANOVA; n=8 for all conditions).

**h.** Survival until IACUC-defined endpoint is increased in mice bearing *Ccr2*$^{-/-}$ cancer cells regardless of the genotype of the host (Log-rank [Mantel-Cox] test; n=8 for all conditions).

**Fig. 2: Loss of CCR2 increases apoptosis *in vivo* with no effect on proliferation**

**a.** Four representative photomicrographs of H&E-stained tumors from *Ccr2*$^{+/+}$ and *Ccr2*$^{-/-}$ cancer cells. Arrows denote cystic areas; also note lipid vacuoles in tumors from *Ccr2*$^{-/-}$ cancer cells (Scale bar=100 μm).

**b.** Histology score of solid area in tumors from *Ccr2*$^{+/+}$ and *Ccr2*$^{-/-}$ transplants (mean +/- SEM, Student's t-test; n=10 in *Ccr2*$^{+/+}$ and n=8 in *Ccr2*$^{-/-}$).

**c.** Proliferation is unchanged between *Ccr2*$^{+/+}$ and *Ccr2*$^{-/-}$ tumor transplants during the growth-restricted phase, (5-6 weeks after transplantation) as determined by Ki67- positive nuclear stain. Left panels are representative photomicrographs (Scale bar=100 μm), and right panel shows quantification (mean +/- SEM, Student's t-test; n=10 and 9 for *Ccr2*$^{+/+}$ and *Ccr2*$^{-/-}$ transplants, respectively).

**d.** Proliferation is unchanged in *Ccr2*$^{+/+}$ and *Ccr2*$^{-/-}$ cancer cells *in vitro* during the growth-restricted phase, as determined by absorbance after 24 h using CellTiter 96 AQueous One Solution Cell Proliferation (MTS) Assay (mean +/- SEM, Student's t-test; n=4).

**e.** *Ccr2*$^{-/-}$ cancer cells have an increased apoptotic index compared to *Ccr2*$^{-/-}$ cancer cells during growth-restricted phase, as determined by double staining for PyMT and cleaved caspase-3. Left panels are representative photomicrographs, with arrows indicating apoptotic cancer cells (scale bar=100 μm),

and right panel shows quantification (mean +/- SEM, Student's t-test; n=5. Each dot represents average from five random views of one tumor).

**f.** *Ccr2*$^{-/-}$ cancer cells are less viable than *Ccr2*$^{+/+}$ cancer cells in serum-free conditions, as determined by absorbance in MTS assay after serum starvation for 24 h (mean +/- SEM, Student's t-test; n=3).

**Fig. 3: *Ccr2*$^{-/-}$ cancer cells have increased expression of interferon (IFN) response genes and of genes involved in MHC class I antigen presentation**

**a.** A hierarchically clustered heat map of *Ccr2*$^{+/+}$ and *Ccr2*$^{-/-}$ cancer cell samples during the growth-restricted phase, based on expression levels of select genes associated with antigen processing and presentation, as well as epithelial-to-mesenchymal transition (n=3).

**b.** Gene set enrichment analysis plots showing enrichment of IFN response and luminal gene set expression in *Ccr2*$^{-/-}$ cancer cells (NES=normalized enrichment score)

**c.** Gene ontology (GO) term enrichment plots showing the most significantly overrepresented GO terms in *Ccr2*$^{-/-}$ cancer cells compared to *Ccr2*$^{+/+}$ cancer cells.

**Fig. 4: Tumors derived from *Ccr2*$^{-/-}$ cancer cells have increased infiltration of activated CTLs**

**a.** Tumors from *Ccr2*$^{-/-}$ cancer cells have fewer CD4+ T cells and more CD8+ T cells during the growth-restricted phase, as determined by flow cytometry gated on CD45+CD3+ cells. Left panels are representative examples of dot plots, and right panels show quantification of CD4+ and CD8+ cells (mean +/- SEM, Student's t-test; n=5).

**b.** Representative immunofluorescence staining showing that more CD8a+ T cells (red) infiltrate into tumors derived from *Ccr2*$^{-/-}$ cancer cells than tumors from *Ccr2*$^{+/+}$ cancer cells during the growth-restricted phase (Scale bar=100 μm).

**c.** Quantification of CD8a+ T cells in the tumors (mean +/- SEM, Student's t-test; n=5 tumors. Each dot represents the average of five random views of one tumor).

**d.** PD-1 levels were increased in CD8+ T cells in tumors from *Ccr2*$^{-/-}$ cancer cells during the growth-restricted phase, as determined by flow cytometry gated on CD45+CD3+CD8+ cells (mean +/- SEM, Student's t-test; n=5).

**e.** LAMP-1 (CD107a) levels were increased in CD8+ T cells in *Ccr2*$^{-/-}$ tumors during the growth-restricted phase, as determined by flow cytometry gated on CD45+CD3+CD8+ cells (mean +/- SEM, Student's t-test; n=4 and 5 for *Ccr2*$^{+/+}$ and *Ccr2*$^{-/-}$ transplants, respectively).

**f.** Intracellular Granzyme B levels were decreased in CD8+ T cells in *Ccr2*$^{-/-}$ tumors during the growth-restricted phase, as determined by flow cytometry gated on CD45+CD3+CD8+ cells, after 2 h of incubation with Brefeldin A (mean +/- SEM, Student's t-test; n=5).

**Fig. 5: Cancer cell CCR2 tumor growth requires functional adaptive immunity**

**a.** Schematic of experimental design.

**b.** Tumors from *Ccr2*$^{+/+}$ cancer cells grow faster than tumors from *Ccr2*$^{-/-}$ cancer cells in mice with intact immune systems. Tumor burden was determined by weekly caliper measurement. Mice were sacrificed at IACUC-approved endpoint (mean +/- SEM, two-way ANOVA; n=20 per condition).

**c.** Tumors from *Ccr2*$^{+/+}$ cancer cells grow similar to tumors from *Ccr2*$^{-/-}$ cancer cells in athymic host mice. Tumor burden was determined by weekly caliper measurement. Mice were sacrificed at IACUC-approved endpoint (mean +/- SEM, two-way ANOVA; n=20 per condition).

**d.** Apoptosis was unchanged between *Ccr2*$^{+/+}$ and *Ccr2*$^{-/-}$ transplants to *Nu/Nu* nude hosts, as determined by TUNEL stain. Left panels are representative photomicrographs (Scale bar=100 μm),

with arrows pointing to apoptotic cells; right panel shows quantification (mean +/- SEM, Student's t-test; n=8 and 6 for *Ccr2*$^{+/+}$ and *Ccr2*$^{-/-}$ transplants, respectively).

**e.** Representative H&E staining of transplanted tumors from *Ccr2*$^{+/+}$ and *Ccr2*$^{-/-}$ cancer cells to nude hosts. Arrows indicate highly necrotic areas (Scale bar=100 μm).

**f.** Histology score of solid area of transplanted tumors from *Ccr2*$^{+/+}$ and *Ccr2*$^{-/-}$ cancer cells to *Nu/Nu* hosts (mean +/- SEM, Student's t-test; n=10 in *Ccr2*$^{+/+}$ and n=9 in *Ccr2*$^{-/-}$).

**Fig. 6: Cancer cell *Ccr2* signaling protects against T cell-mediated killing**

**a.** Primary tumor growth is reduced in MMTV-PyMT-chOVA;*Ccr2*$^{-/-}$ mice compared to MMTV-PyMT;*Ccr2*$^{+/+}$ mice, as determined by weekly caliper measurement once the tumors were palpable (mean +/- SEM, two-way ANOVA; n=6 MMTV-PyMT;*Ccr2*$^{+/+}$, and n=5 MMTV-PyMT;*Ccr2*$^{-/-}$ mice).

**b.** *Ccr2*$^{-/-}$ cancer cells are more sensitive to T cell cytotoxicity than *Ccr2*$^{+/+}$ cancer cells. Cytotoxicity of CD8+ OT-1 T cells toward MMTV-PyMT-chOVA;*Ccr2*$^{+/+}$ or MMTV-PyMT-chOVA;*Ccr2*$^{-/-}$ primary cancer cells, with or without OVA peptides, measured by chromium ($Cr^{51}$) release (mean +/- SEM, Student's t-test; n=3).

**c.** Inhibiting CCR2 increased T cell cytotoxicity against *Ccr2*$^{+/+}$ cancer cells. Cytotoxicity of CD8+ OT-1 T cells toward MMTV-PyMT-chOVA;*Ccr2*$^{+/+}$ or MMTV-PyMT-chOVA;*Ccr2*$^{-/-}$ cancer cells, with or without CCR2 inhibitor, measured by chromium ($Cr^{51}$) release (mean +/- SEM, Student's t-test; each dot is the average of triplicate from an independent experiment. n=4 and 3 for MMTV-PyMT-chOVA;*Ccr2*$^{+/+}$ and MMTV-PyMT-chOVA;*Ccr2*$^{-/-}$ cancer cells, respectively).

**d.** Model of clonality measured by T cell receptor (TCR) sequencing.

**e.** Productive clonality in tumors from *Ccr2*$^{+/+}$ and *Ccr2*$^{-/-}$ cancer cells (mean +/- SEM, Student's t-test; n=4).

**f.** Productive clonality in spleens was unchanged between *Ccr2*$^{+/+}$ and *Ccr2*$^{-/-}$ tumors (mean +/- SEM, Student's t-test; n=4).

**Fig. 7: Localized STAT1 activation in *Ccr2*$^{-/-}$ tumors**

**a.** Comparison of STAT1 activation in tumors from *Ccr2*$^{+/+}$ or *Ccr2*$^{-/-}$ cancer cells during the growth-restricted phase, by Western blot analysis (left). Quantifications of protein expression normalized to β-actin levels (right) (mean +/- SEM).

**b.** Representative photomicrographs of p-STAT1 (top) and p-STAT3 (bottom) staining in sections of tumors from *Ccr2*$^{+/+}$ or *Ccr2*$^{-/-}$ cancer cells. Scale bar=100 μm.

**c.** Quantification of the immunohistochemical staining in (b), using H-score, shows higher STAT1 phosphorylation in tumors from *Ccr2*$^{-/-}$ than from *Ccr2*$^{+/+}$ cancer cells, but similar levels of STAT3 phosphorylation (mean +/- SEM, Student's t-test; n= 5).

**Fig. 8: MHC class I expression is reduced and PD-L1 expression increased in *Ccr2*$^{+/+}$ cancer cells in immune competent mice**

**a.** MHC class I expression is increased in MMTV-PyMT-chOVA;*Ccr2*$^{-/-}$ tumors compared to MMTV-PyMT-chOVA;*Ccr2*$^{+/+}$ tumors during the growth-restricted phase, as determined by immunofluorescence staining (upper panels; Scale bar=50 μm) and by flow cytometry (bottom panel), gated on EpCAM+, mCherry+ cells (mean +/- SEM, Student's t-test; n=8 and 4 for PyMT-chOVA;*Ccr2*$^{+/+}$ and PyMT-chOVA;*Ccr2*$^{-/-}$ tumors, respectively).

**b.** MHC class I is increased on *Ccr2*$^{-/-}$ compared to *Ccr2*$^{+/+}$ cancer cells after transplantation into C57BL/6 hosts during the growth-restricted phase, as determined by immunofluorescence staining (upper panels; Scale bar=50 μm). Quantification of mean pixel count (bottom panel, mean +/- SEM, Student's t-test; n= 5)

**c.** MHC class I is unchanged on *Ccr2*$^{+/+}$ and *Ccr2*$^{-/-}$ transplants to *Nu/Nu* hosts, as determined by immunofluorescence staining (upper panels; Scale bar=50 μm). Quantification of mean pixel count (bottom panel, mean +/- SEM, Student's t-test; n=4 and 5 for *Ccr2*$^{+/+}$ and *Ccr2*$^{-/-}$ transplants, respectively).

**d.** PD-L1 is decreased on *Ccr2*$^{-/-}$ cancer cells, as determined by flow cytometry gated on EpCAM+ cells (mean +/- SEM, Student's t-test; n=5).

**e.** PD-L1 mRNA levels are decreased on cultured *Ccr2*$^{-/-}$ cancer cells but respond equally well to IFN-γ treatment, as determined by qPCR. *Ccr2*$^{+/+}$ and *Ccr2*$^{-/-}$ cancer cells growing in culture were treated with either 0, 0.2, 2.0, or 20 ng/mL of recombinant IFN-γ for 48 h (mean +/- SEM, Student's t-test; n=3).

**f.** Treatment with four intraperitoneal doses of anti-PD-L1 antibody (200 μg/injection) had no significant effect on growth of *Ccr2*$^{+/+}$ or *Ccr2*$^{-/-}$ tumors *in vivo*, compared to control rat IgG antibody (arrows indicate treatments; mean +/- SEM, two-way ANOVA; n=20 for all conditions).

**Fig. 9: *Ccr2*$^{-/-}$ tumors promote infiltration and activation of cross-presenting CD103+ DCs**

**a.** Representative immunofluorescence stainings showing that more CD11c+ dendritic cells (red) infiltrate into *Ccr2*$^{-/-}$ tumors compared to *Ccr2*$^{+/+}$ tumors during the growth-restricted phase (EpCAM+, green; Scale bar=100 μm).

**b.** CD103+ DCs are increased in *Ccr2*$^{-/-}$ tumors compared to *Ccr2*$^{+/+}$ tumors during the growth-restricted phase, as determined by flow cytometry gated on CD45+CD11c+MHC class II+ cells. SSC=side scatter (mean +/- SEM, Student's t-test; n=5).

**c.** CD103+ DCs are increased in the draining lymph nodes (dLNs) of *Ccr2*$^{-/-}$ tumors compared to the dLNs of *Ccr2*$^{+/+}$ tumors during the growth-restricted phase, as determined by flow cytometry gated on CD45+CD11c+MHC class II+ cells (mean +/- SEM, Student's t-test; n=5).

**d.** Tumors from transplanted *Ccr2*$^{-/-}$ cancer cells have increased DC infiltration and elevated markers of DC activation compared to tumors from *Ccr2*$^{+/+}$ cancer cells. Real-time PCR on tumors during the growth-restricted phase for *Ccr2*$^{+/+}$ and *Ccr2*$^{-/-}$ tumors (mean +/- SEM, Student's t-test; For *Cd11c*, n=6 in *Ccr2*$^{+/+}$ and n=8 in *Ccr2*$^{-/-}$ , For all other TR-PCR results: n=5 in *Ccr2*$^{+/+}$ and n=6 in *Ccr2*$^{-/-}$).

**e.** DCs in *Ccr2*$^{-/-}$ tumors are more activated during the growth-restricted phase, as determined by flow cytometry for CD86+ gated on CD45+CD11c+MHC class II+ cells (mean +/- SEM, Student's t-test; n=5).

**f.** Flow cytometry on dLNs with or without injection of irradiated cancer cells. Note that CD103+ DCs are only increased in the dLNs of the glands after injection of *Ccr2*$^{-/-}$ cancer cells, not in non-dLNs from axillary glands (mean +/- SEM, Student's t-test; n=5).

**g.** CD103+ DCs are decreased in *Ccr2*$^{-/-}$ tumors compared to *Ccr2*$^{+/+}$ tumors in *Nu/Nu* hosts, as determined by flow cytometry gated on CD45+CD11c+ cells (mean +/- SEM, Student's t-test; n=5).

**Fig. 10: Cross-presenting CD103+ DCs are critical for immune control of *Ccr2*$^{-/-}$ cancer cells**

**a.** Conditioned medium from *Ccr2*$^{-/-}$ cancer cells induced similar numbers of CD11c DCs (left), but more CD103+ BMDCs (right) *in vitro*, compared to conditioned medium from *Ccr2*$^{+/+}$ cancer cells (mean +/- SEM, Student's t-test; n=3).

**b.** Conditioned medium from *Ccr2*$^{+/+}$ cancer cells cultured with CCR2 antagonist induced similar numbers of CD11c DCs (left), but more CD103+ BMDCs (right) *in vitro* than conditioned medium from control cells cultured in normal culture medium (mean +/- SEM, Student's t-test; n=3).

**c.** Tumors from transplanted *Ccr2*$^{-/-}$ cancer cells have elevated *Csf2* mRNA (coding GM-CSF) and *Flt3l* (coding FLT3 ligand), but not *Ccl2* or *Csf3* compared to tumors from *Ccr2*$^{+/+}$ cancer cells. Real-time PCR on *Ccr2*$^{+/+}$ and *Ccr2*$^{-/-}$ transplanted tumors during the growth-restricted phase (mean +/- SEM, Student's t-test; n=5-6 *Ccr2*$^{+/+}$ tumors and n=6 *Ccr2*$^{-/-}$ tumors).

**d.** Tumor growth is increased in *Batf3*$^{-/-}$ hosts transplanted with *Ccr2*$^{-/-}$ cancer cells, as determined by weekly caliper measurement (mean +/- SEM, two-way ANOVA; n=9 in *Ccr2*$^{+/+}$ to *Batf3*$^{-/-}$ hosts group, and n=10 for the other 3 groups)

**e.** CD103+ DCs are increased in *Ccr2*$^{-/-}$ tumors compared to *Ccr2*$^{+/+}$ tumors in C57BL/6 hosts but are low in *Batf3*$^{-/-}$ hosts (mean +/- SEM, Student's t-tests; n=5).

**f.** CD8a+ T cells are increased in early-stage tumors (3 weeks) from transplanted *Ccr2*$^{-/-}$ cancer cells compared to tumors from *Ccr2*$^{+/+}$ cancer cells in C57BL/6 hosts, but are low in *Batf3*$^{-/-}$ hosts (mean +/- SEM, Student's t-tests; n=9-10).

**g.** Lamp-1 (CD107a) and CD8a double-positive T cells were increase in early-stage tumors (3 weeks) from transplanted *Ccr2*$^{-/-}$ cancer cells compared to tumors from *Ccr2*$^{+/+}$ cancer cells but are low in *Batf3*$^{-/-}$ hosts (mean +/- SEM, Student's t-tests; n=9-10).

**h.** PD-1 and CD8a double-positive T cells were increased in early-stage tumors (3 weeks) from transplanted *Ccr2*$^{-/-}$ cancer cells compared to tumors from *Ccr2*$^{+/+}$ cancer cells in C57BL/6 hosts, but are low in *Batf3*$^{-/-}$ hosts (mean +/- SEM, Student's t-tests; n=5).

**i.** Model of how cancer cell CCR2 orchestrates immune suppression.

# Figure 1

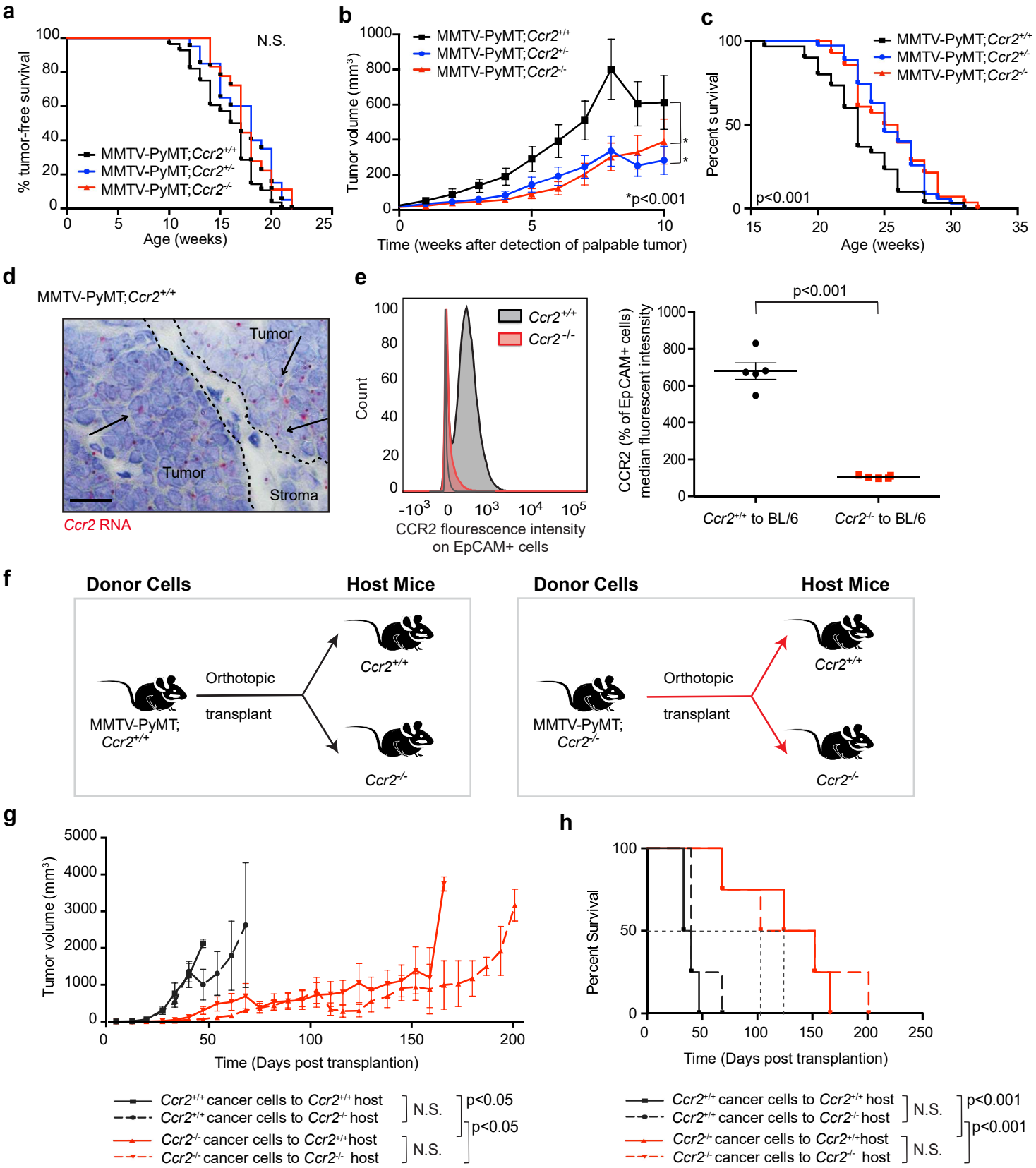
a
% tumor-free survival
N.S.
MMTV-PyMT;Ccr2+/+
MMTV-PyMT;Ccr2+/-
MMTV-PyMT;Ccr2-/-
Age (weeks)
b
Tumor volume (mm3)
*p<0.001
Time (weeks after detection of palpable tumor)
c
Percent survival
p<0.001
Age (weeks)
d
MMTV-PyMT;Ccr2+/+
Tumor
Stroma
Ccr2 RNA
e
Count
Ccr2+/+
Ccr2-/-
CCR2 flourescence intensity on EpCAM+ cells
p<0.001
CCR2 (% of EpCAM+ cells) median fluorescent intesnsity
Ccr2+/+ to BL/6
Ccr2-/- to BL/6
f
Donor Cells
Host Mice
Orthotopic transplant
MMTV-PyMT; Ccr2+/+
Ccr2+/+
Ccr2-/-
MMTV-PyMT; Ccr2-/-
g
Tumor volume (mm3)
Time (Days post transplantion)
Ccr2+/+ cancer cells to Ccr2+/+ host
Ccr2+/+ cancer cells to Ccr2-/- host
Ccr2-/- cancer cells to Ccr2+/+host
Ccr2-/- cancer cells to Ccr2-/- host
N.S.
p<0.05
h
Percent Survival
Time (Days post transplantion)
p<0.001

## Figure 2

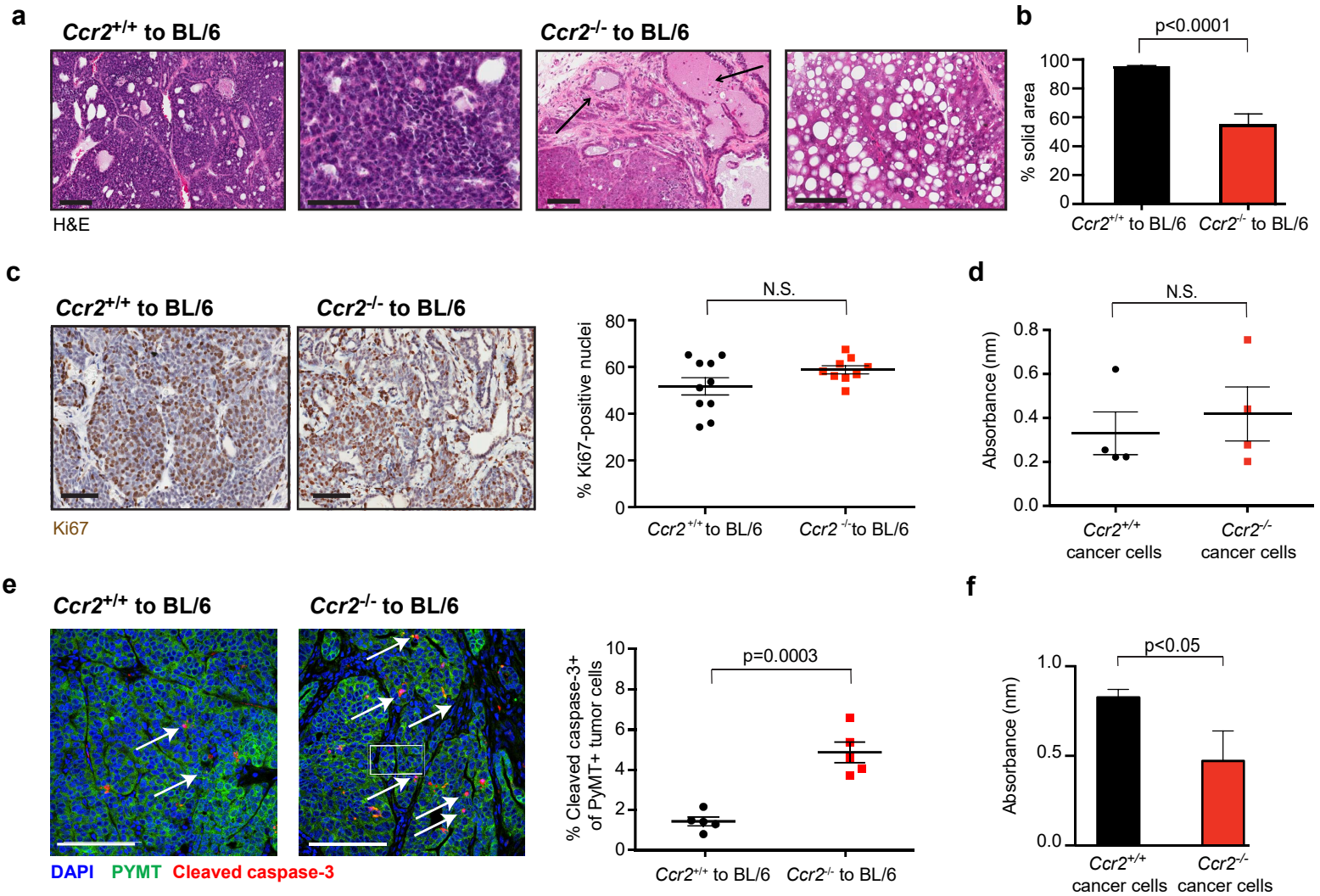
a
Ccr2+/+ to BL/6
Ccr2-/- to BL/6
H&E
b
p<0.0001
% solid area
100
80
60
40
20
0
Ccr2+/+ to BL/6
Ccr2-/- to BL/6
c
Ccr2+/+ to BL/6
Ccr2-/- to BL/6
Ki67
N.S.
% Ki67-positive nuclei
80
60
40
20
0
Ccr2+/+ to BL/6
Ccr2-/- to BL/6
d
N.S.
Absorbance (nm)
0.8
0.6
0.4
0.2
0.0
Ccr2+/+ cancer cells
Ccr2-/- cancer cells
e
Ccr2+/+ to BL/6
Ccr2-/- to BL/6
DAPI PYMT Cleaved caspase-3
p=0.0003
% Cleaved caspase-3+ of PyMT+ tumor cells
10
8
6
4
2
0
Ccr2+/+ to BL/6
Ccr2-/- to BL/6
f
p<0.05
Absorbance (nm)
1.0
0.5
0.0
Ccr2+/+ cancer cells
Ccr2-/- cancer cells

**Figure 3**

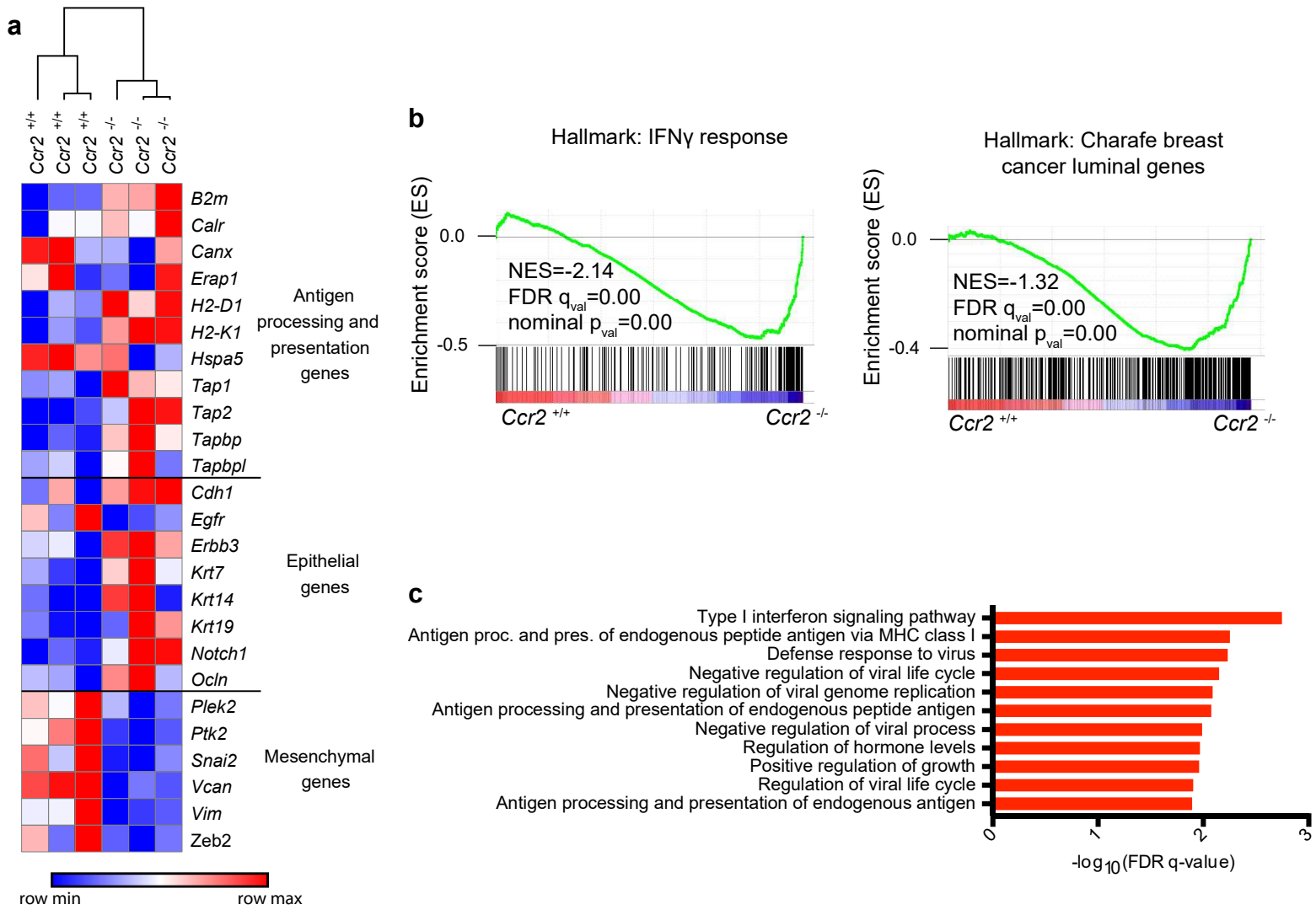
a
Ccr2 +/+
Ccr2 +/+
Ccr2 +/+
Ccr2 -/-
Ccr2 -/-
Ccr2 -/-
B2m
Calr
Canx
Erap1
H2-D1
H2-K1
Hspa5
Tap1
Tap2
Tapbp
Tapbpl
Antigen processing and presentation genes
Cdh1
Egfr
Erbb3
Krt7
Krt14
Krt19
Notch1
Ocln
Epithelial genes
Plek2
Ptk2
Snai2
Vcan
Vim
Zeb2
Mesenchymal genes
row min
row max
b
Hallmark: IFNγ response
Enrichment score (ES)
0.0
-0.5
NES=-2.14
FDR q_val=0.00
nominal p_val=0.00
Ccr2 +/+
Ccr2 -/-
Hallmark: Charafe breast cancer luminal genes
Enrichment score (ES)
0.0
-0.4
NES=-1.32
FDR q_val=0.00
nominal p_val=0.00
Ccr2 +/+
Ccr2 -/-
c
Type I interferon signaling pathway
Antigen proc. and pres. of endogenous peptide antigen via MHC class I
Defense response to virus
Negative regulation of viral life cycle
Negative regulation of viral genome replication
Antigen processing and presentation of endogenous peptide antigen
Negative regulation of viral process
Regulation of hormone levels
Positive regulation of growth
Regulation of viral life cycle
Antigen processing and presentation of endogenous antigen
0
1
2
3
-log10(FDR q-value)

## Figure 4

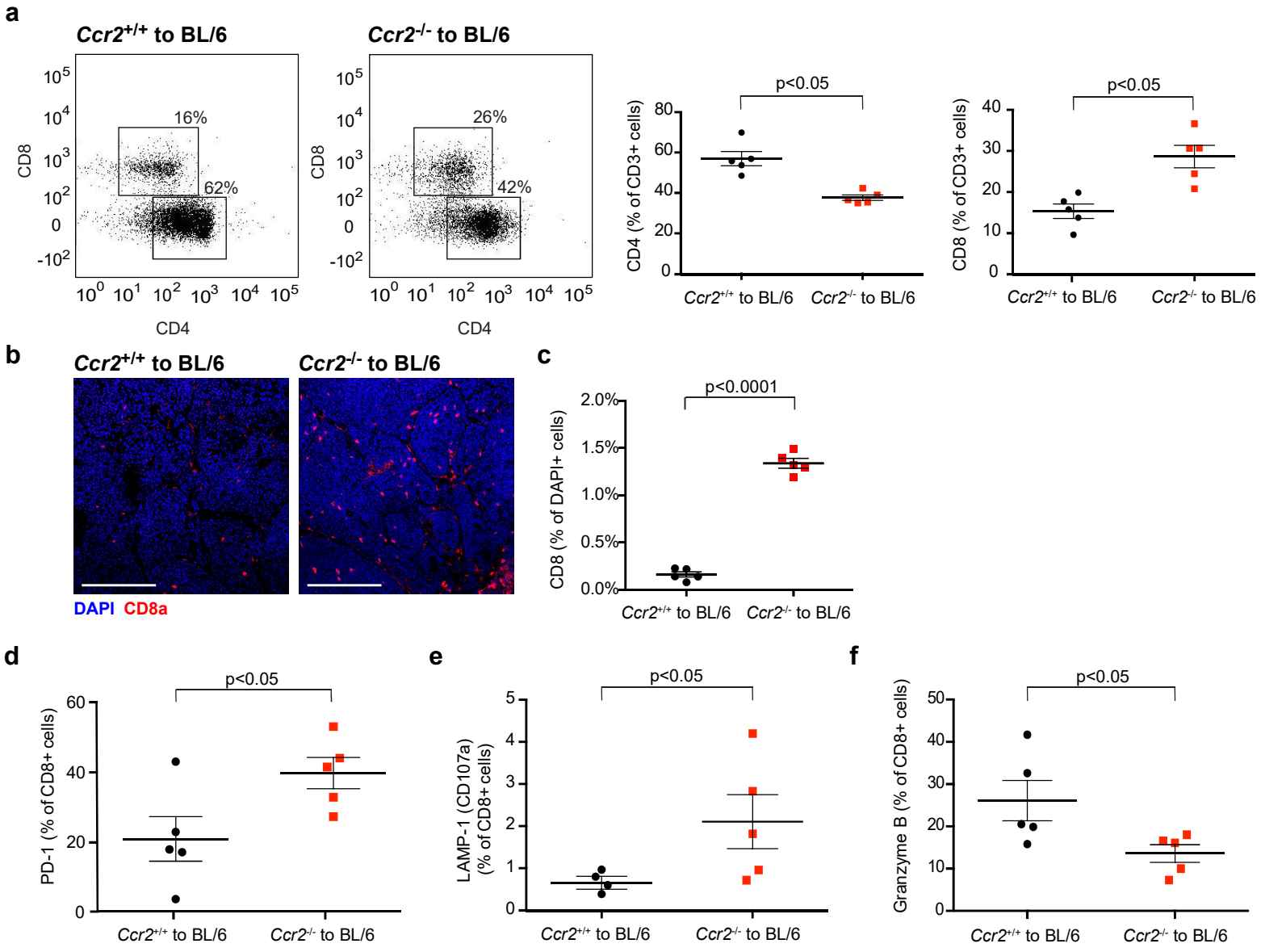
a
Ccr2+/+ to BL/6
Ccr2-/- to BL/6
CD8
CD4
16%
62%
26%
42%
p<0.05
CD4 (% of CD3+ cells)
CD8 (% of CD3+ cells)
b
DAPI CD8a
c
p<0.0001
CD8 (% of DAPI+ cells)
d
PD-1 (% of CD8+ cells)
e
LAMP-1 (CD107a) (% of CD8+ cells)
f
Granzyme B (% of CD8+ cells)

**Figure 5**

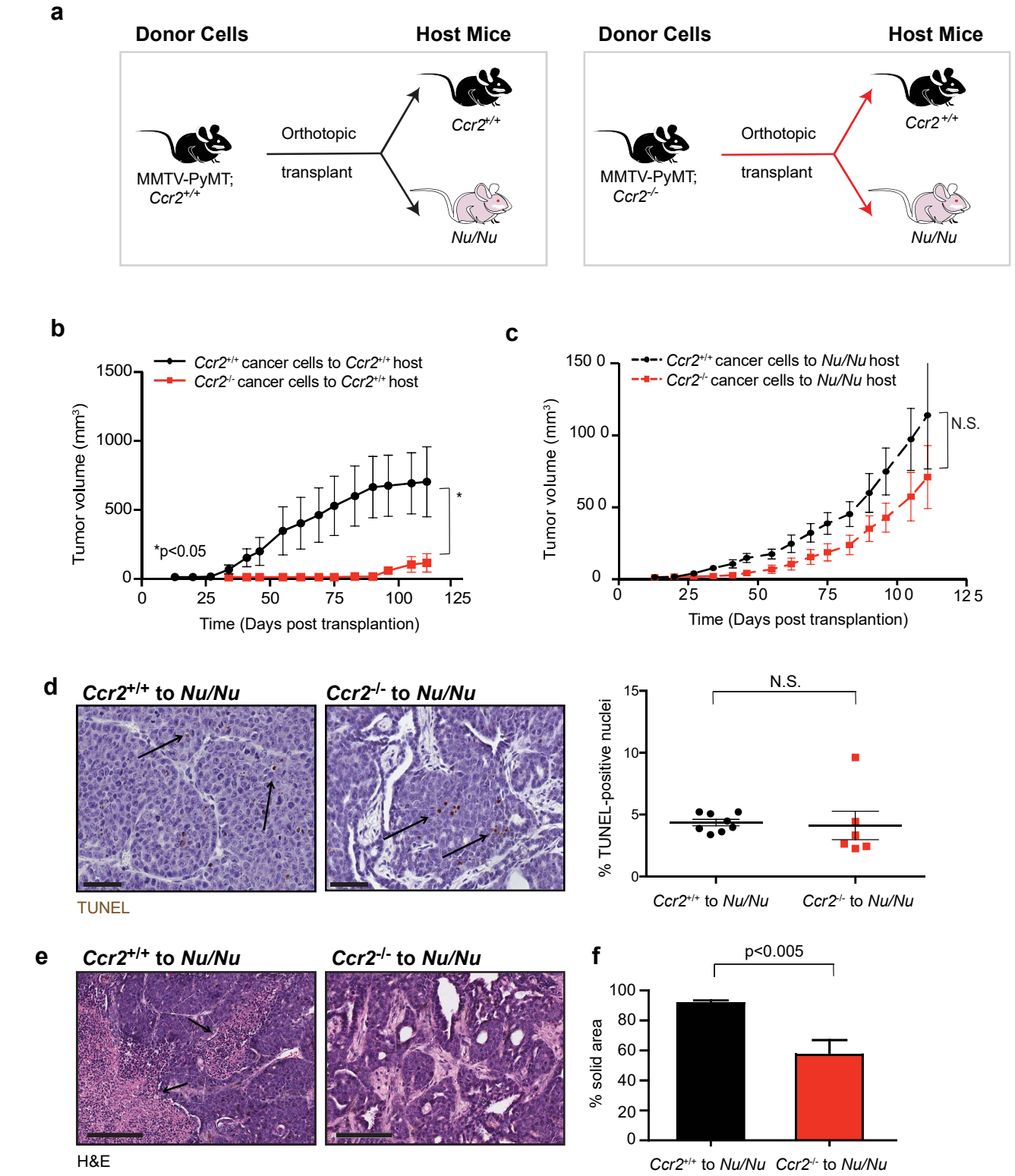
a
Donor Cells
Host Mice
MMTV-PyMT; Ccr2+/+
Orthotopic transplant
Ccr2+/+
Nu/Nu
Donor Cells
Host Mice
MMTV-PyMT; Ccr2-/-
Orthotopic transplant
Ccr2+/+
Nu/Nu
b
Ccr2+/+ cancer cells to Ccr2+/+ host
Ccr2-/- cancer cells to Ccr2+/+ host
Tumor volume (mm3)
1500
1000
500
0
*p<0.05
*
0
25
50
75
100
125
Time (Days post transplantion)
c
Ccr2+/+ cancer cells to Nu/Nu host
Ccr2-/- cancer cells to Nu/Nu host
Tumor volume (mm3)
150 0
100 0
50 0
0
N.S.
0
25
50
75
100
125
Time (Days post transplantion)
d
Ccr2+/+ to Nu/Nu
Ccr2-/- to Nu/Nu
TUNEL
N.S.
% TUNEL-positive nuclei
15
10
5
0
Ccr2+/+ to Nu/Nu
Ccr2-/- to Nu/Nu
e
Ccr2+/+ to Nu/Nu
Ccr2-/- to Nu/Nu
H&E
f
p<0.005
% solid area
100
80
60
40
20
0
Ccr2+/+ to Nu/Nu
Ccr2-/- to Nu/Nu

# Figure 6

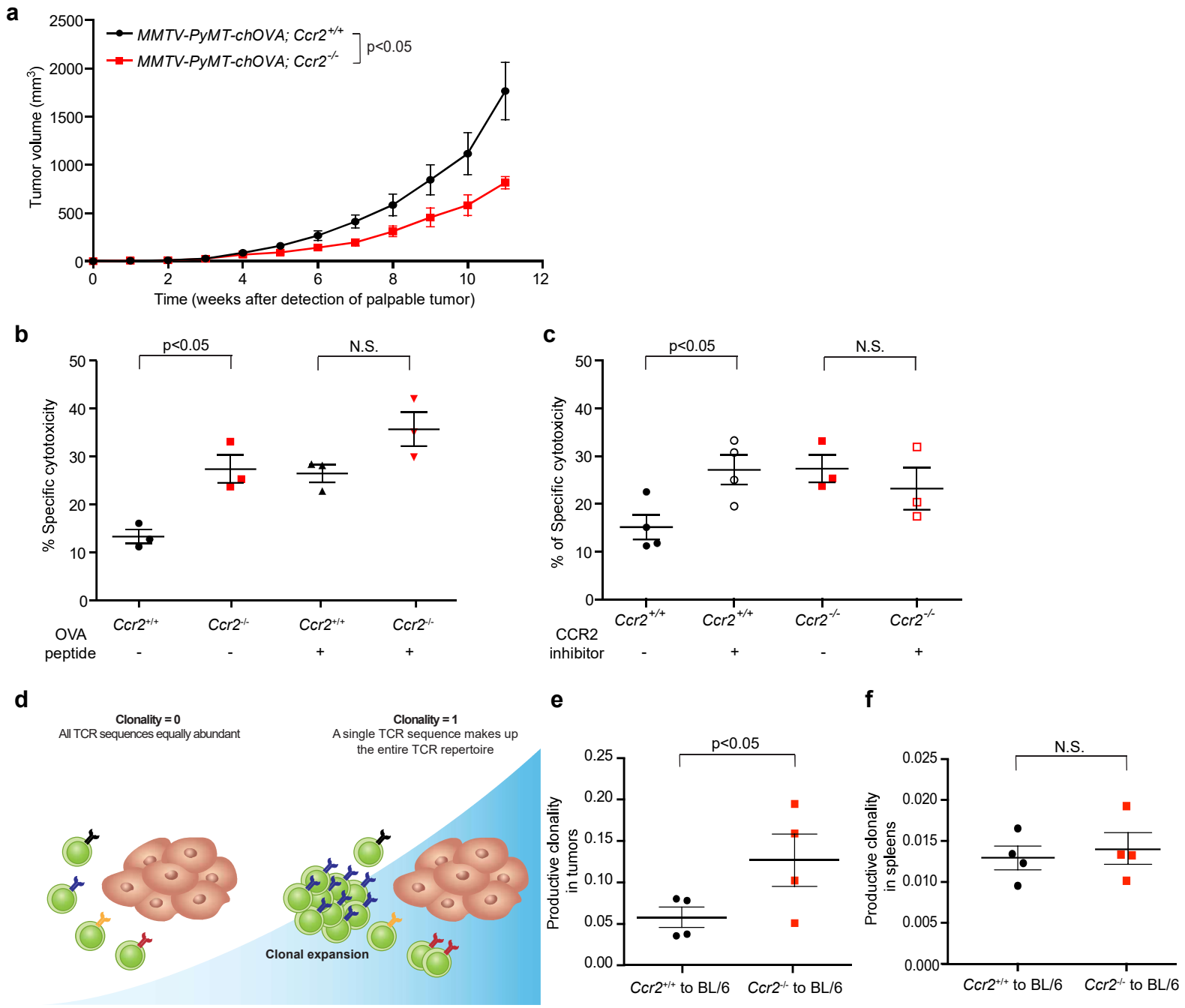
a
MMTV-PyMT-chOVA; Ccr2+/+
MMTV-PyMT-chOVA; Ccr2-/-
p<0.05
Tumor volume (mm3)
Time (weeks after detection of palpable tumor)
b
p<0.05
N.S.
% Specific cytotoxicity
Ccr2+/+
Ccr2-/-
OVA peptide
c
% of Specific cytotoxicity
CCR2 inhibitor
d
Clonality = 0
All TCR sequences equally abundant
Clonality = 1
A single TCR sequence makes up the entire TCR repertoire
Clonal expansion
e
Productive clonality in tumors
Ccr2+/+ to BL/6
Ccr2-/- to BL/6
f
Productive clonality in spleens

**Figure 7**

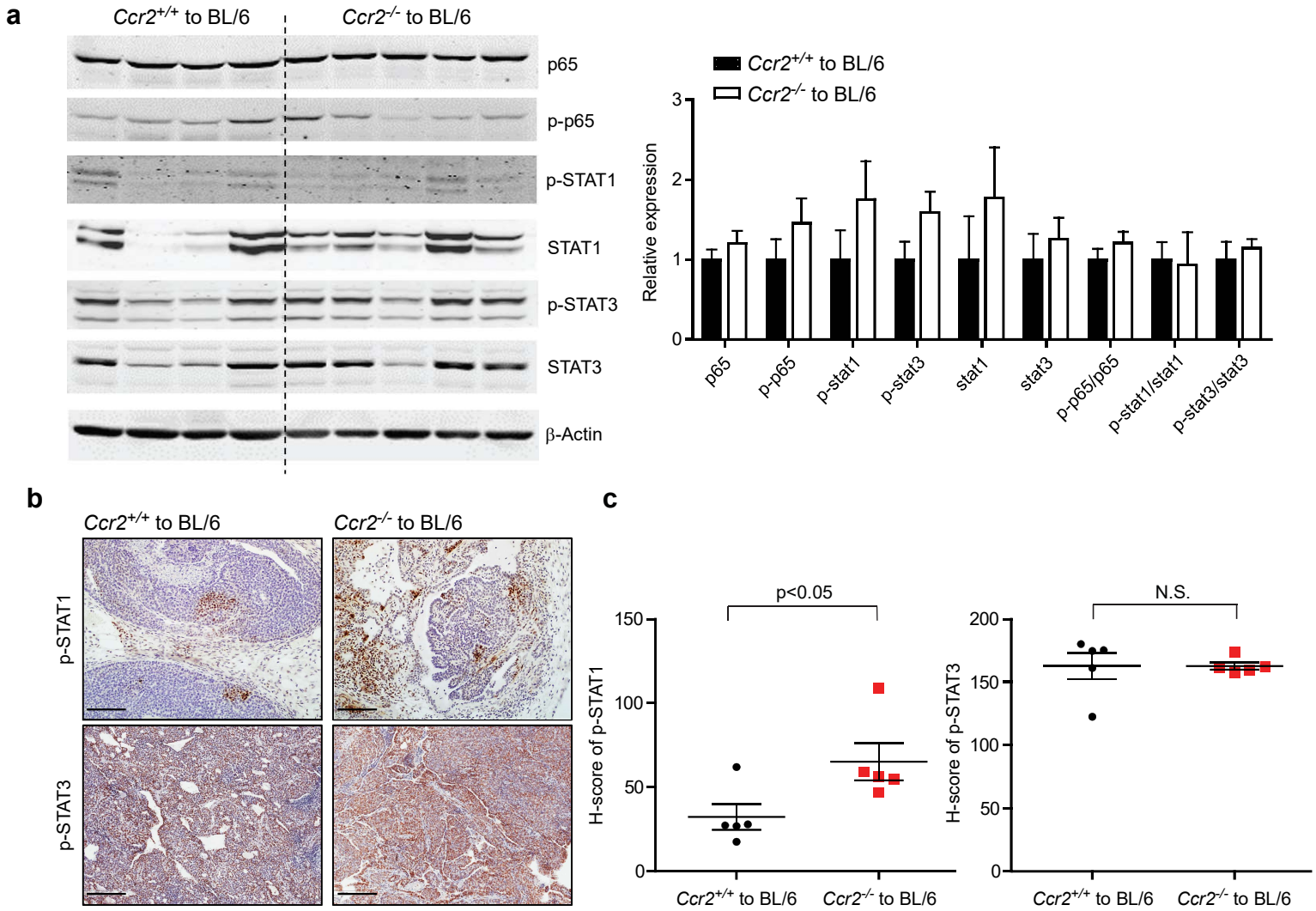
a
Ccr2+/+ to BL/6
Ccr2-/- to BL/6
p65
p-p65
p-STAT1
STAT1
p-STAT3
STAT3
β-Actin
Ccr2+/+ to BL/6
Ccr2-/- to BL/6
Relative expression
0
1
2
3
p65
p-p65
p-stat1
p-stat3
stat1
stat3
p-p65/p65
p-stat1/stat1
p-stat3/stat3
b
Ccr2+/+ to BL/6
Ccr2-/- to BL/6
p-STAT1
p-STAT3
c
p<0.05
H-score of p-STAT1
0
50
100
150
Ccr2+/+ to BL/6
Ccr2-/- to BL/6
N.S.
H-score of p-STAT3
0
50
100
150
200
Ccr2+/+ to BL/6
Ccr2-/- to BL/6

# Figure 8

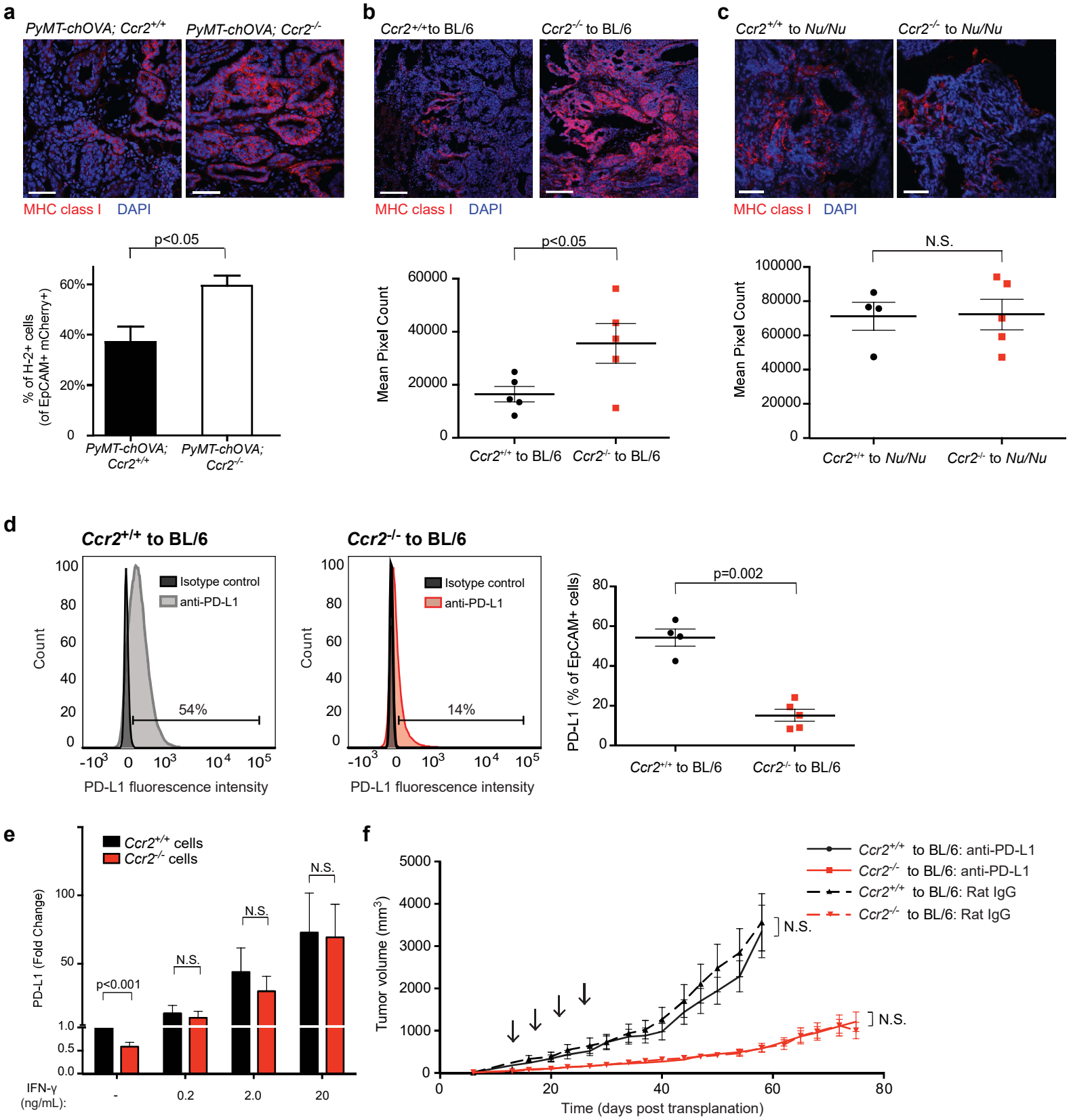
a
PyMT-chOVA; Ccr2+/+
PyMT-chOVA; Ccr2-/-
MHC class I DAPI
p<0.05
% of H-2+ cells (of EpCAM+ mCherry+)
60%
40%
20%
0
PyMT-chOVA; Ccr2+/+
PyMT-chOVA; Ccr2-/-
b
Ccr2+/+to BL/6
Ccr2-/- to BL/6
MHC class I DAPI
p<0.05
Mean Pixel Count
60000
40000
20000
0
Ccr2+/+ to BL/6
Ccr2-/- to BL/6
c
Ccr2+/+ to Nu/Nu
Ccr2-/- to Nu/Nu
MHC class I DAPI
N.S.
Mean Pixel Count
100000
80000
60000
40000
20000
0
Ccr2+/+ to Nu/Nu
Ccr2-/- to Nu/Nu
d
Ccr2+/+ to BL/6
Isotype control
anti-PD-L1
Count
54%
PD-L1 fluorescence intensity
Ccr2-/- to BL/6
Isotype control
anti-PD-L1
Count
14%
PD-L1 fluorescence intensity
p=0.002
PD-L1 (% of EpCAM+ cells)
Ccr2+/+ to BL/6
Ccr2-/- to BL/6
e
Ccr2+/+ cells
Ccr2-/- cells
PD-L1 (Fold Change)
p<0.001
N.S.
N.S.
N.S.
IFN-γ (ng/mL):
-
0.2
2.0
20
f
Ccr2+/+ to BL/6: anti-PD-L1
Ccr2-/- to BL/6: anti-PD-L1
Ccr2+/+ to BL/6: Rat IgG
Ccr2-/- to BL/6: Rat IgG
Tumor volume (mm3)
N.S.
N.S.
Time (days post transplanation)

## Figure 9

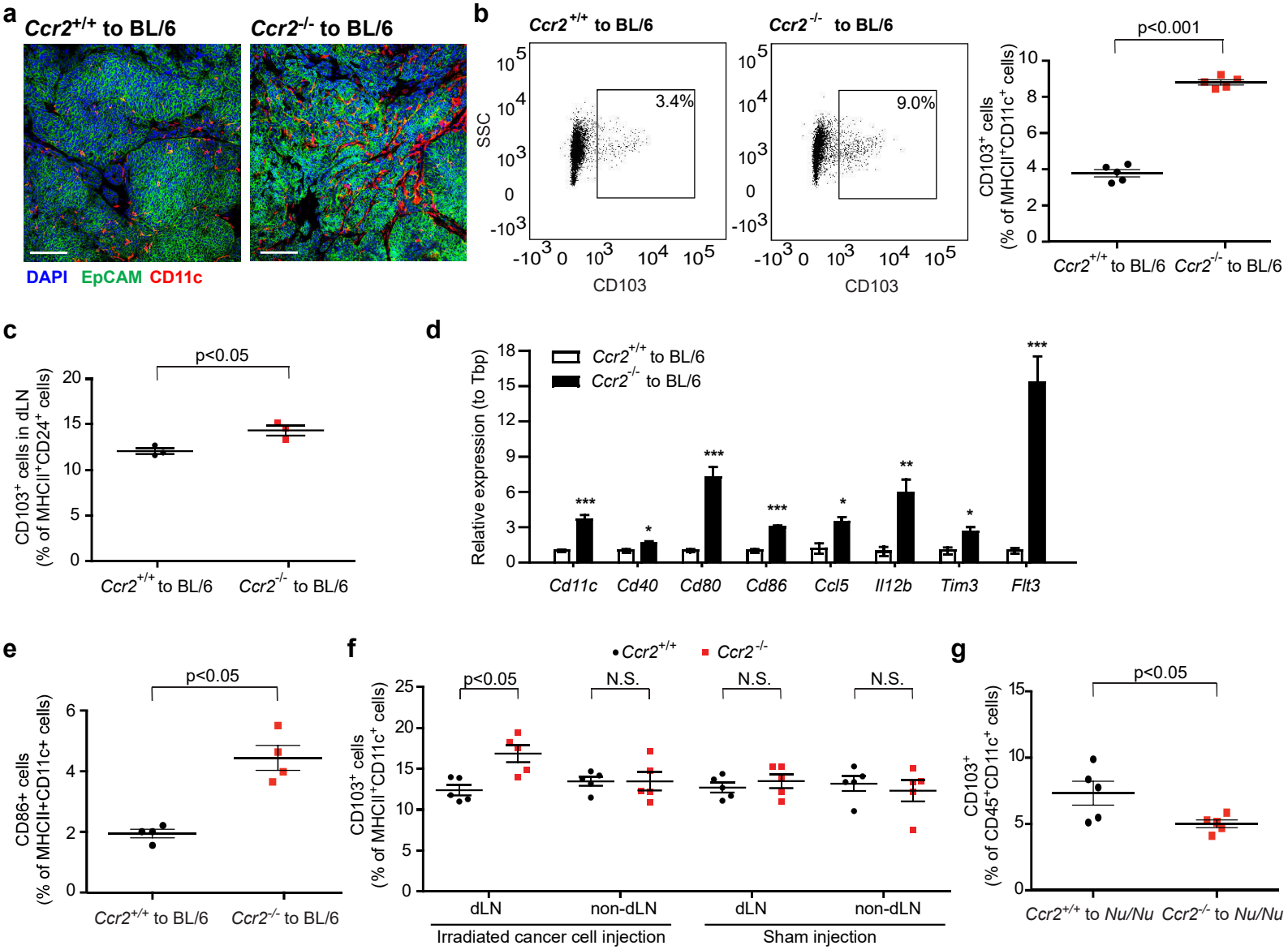
a
Ccr2+/+ to BL/6
Ccr2-/- to BL/6
DAPI EpCAM CD11c
b
Ccr2+/+ to BL/6
Ccr2-/- to BL/6
SSC
CD103
3.4%
9.0%
p<0.001
CD103+ cells (% of MHCII+CD11c+ cells)
Ccr2+/+ to BL/6
Ccr2-/- to BL/6
c
p<0.05
CD103+ cells in dLN (% of MHCII+CD24+ cells)
Ccr2+/+ to BL/6
Ccr2-/- to BL/6
d
Relative expression (to Tbp)
Ccr2+/+ to BL/6
Ccr2-/- to BL/6
Cd11c
Cd40
Cd80
Cd86
Ccl5
Il12b
Tim3
Flt3
e
p<0.05
CD86+ cells (% of MHCII+CD11c+ cells)
Ccr2+/+ to BL/6
Ccr2-/- to BL/6
f
Ccr2+/+
Ccr2-/-
p<0.05
N.S.
N.S.
N.S.
CD103+ cells (% of MHCII+CD11c+ cells)
dLN
non-dLN
dLN
non-dLN
Irradiated cancer cell injection
Sham injection
g
p<0.05
CD103+ (% of CD45+CD11c+ cells)
Ccr2+/+ to Nu/Nu
Ccr2-/- to Nu/Nu

**Figure 10**

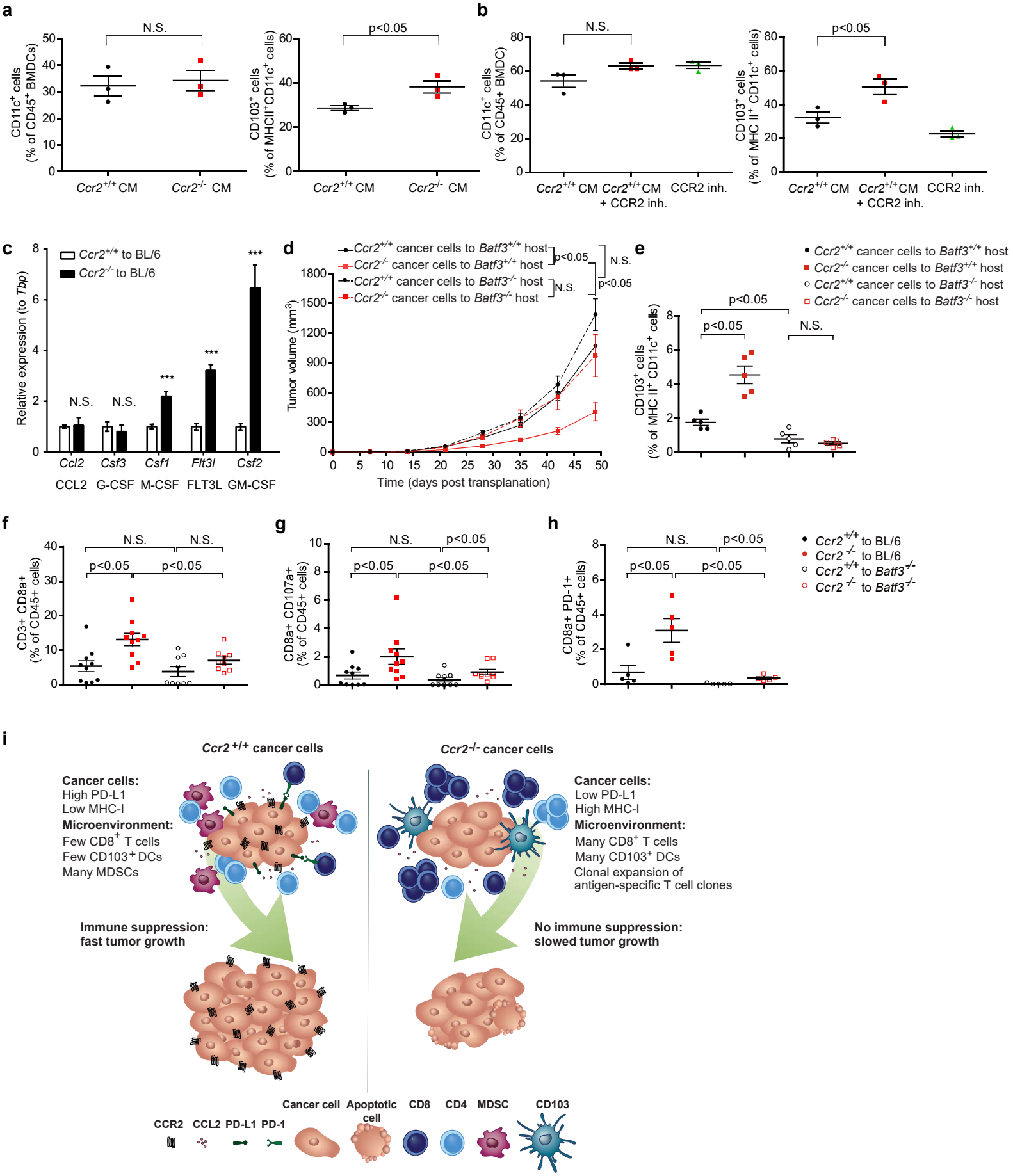
a
N.S.
p<0.05
CD11c+ cells (% of CD45+ BMDCs)
CD103+ cells (% of MHCII+CD11c+ cells)
Ccr2+/+ CM
Ccr2-/- CM
b
CD11c+ cells (% of CD45+ BMDC)
CD103+ cells (% of MHC II+ CD11c+ cells)
Ccr2+/+ CM
Ccr2+/+ CM + CCR2 inh.
CCR2 inh.
c
Ccr2+/+ to BL/6
Ccr2-/- to BL/6
Relative expression (to Tbp)
N.S.
***
Ccl2
Csf3
Csf1
Flt3l
Csf2
CCL2
G-CSF
M-CSF
FLT3L
GM-CSF
d
Ccr2+/+ cancer cells to Batf3+/+ host
Ccr2-/- cancer cells to Batf3+/+ host
Ccr2+/+ cancer cells to Batf3-/- host
Ccr2-/- cancer cells to Batf3-/- host
p<0.05
N.S.
Tumor volume (mm3)
Time (days post transplanation)
e
CD103+ cells (% of MHC II+ CD11c+ cells)
f
CD3+ CD8a+ (% of CD45+ cells)
g
CD8a+ CD107a+ (% of CD45+ cells)
h
CD8a+ PD-1+ (% of CD45+ cells)
Ccr2+/+ to BL/6
Ccr2-/- to BL/6
Ccr2+/+ to Batf3-/-
Ccr2-/- to Batf3-/-
i
Ccr2+/+ cancer cells
Ccr2-/- cancer cells
Cancer cells:
High PD-L1
Low MHC-I
Microenvironment:
Few CD8+ T cells
Few CD103+ DCs
Many MDSCs
Immune suppression:
fast tumor growth
Cancer cells:
Low PD-L1
High MHC-I
Microenvironment:
Many CD8+ T cells
Many CD103+ DCs
Clonal expansion of antigen-specific T cell clones
No immune suppression:
slowed tumor growth
CCR2
CCL2
PD-L1
PD-1
Cancer cell
Apoptotic cell
CD8
CD4
MDSC
CD103